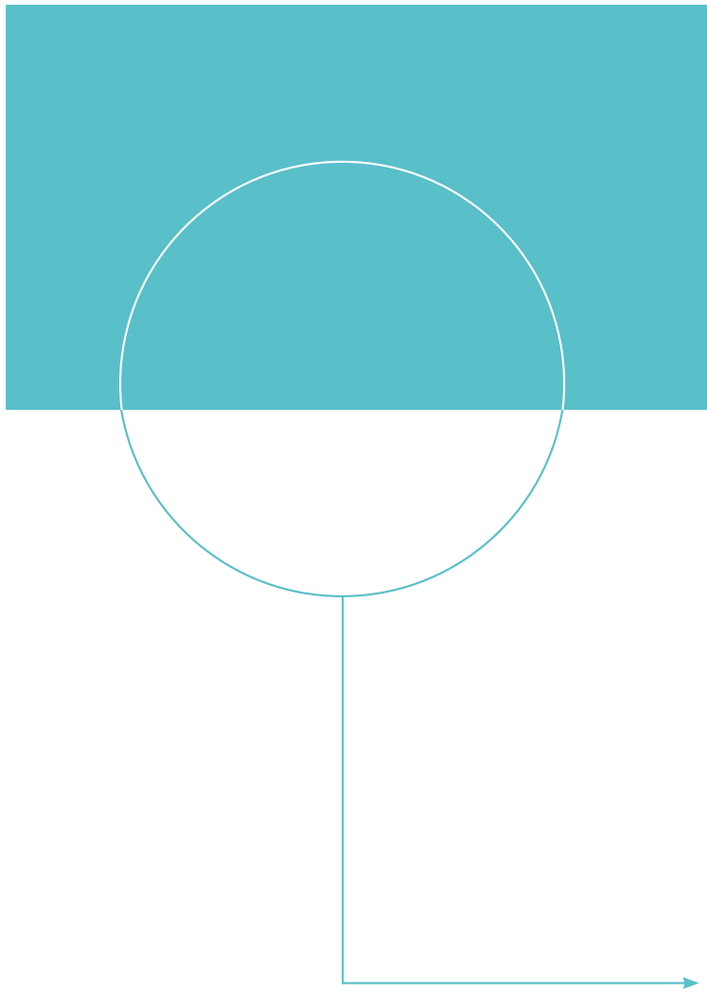

Master's thesis

2019

Sungsoo Lim

**NTNU**
Norwegian University of
Science and Technology
Faculty of Engineering
Department of Civil and Environmental Engineering

Sungsoo Lim

# Numerical Modelling for Fluid-Structure Interaction of Aquaculture Collar Structures using a Beam Model

July 2019

NTNU
Norwegian University of
Science and Technology

NTNU
Norwegian University of
Science and Technology

NTNU

Norwegian University of
Science and Technology

# Numerical Modelling for Fluid-Structure Interaction of Aquaculture Collar Structures using a Beam Model

**Sungsoo Lim**

Coastal and Marine Engineering and Management (CoMEM)
Submission date: July 2019
Supervisor: Hans Bihs
Co-supervisor: Arun Kamath
Tobias Martin

Norwegian University of Science and Technology
Department of Civil and Environmental Engineering

ERASMUS +: ERASMUS MUNDUS MOBILITY PROGRAMME

Master of Science in

COASTAL AND MARINE ENGINEERING AND MANAGEMENT

CoMEM

# NUMERICAL MODELLING FOR FLUID-STRUCTURE INTERACTION OF AQUACULTURE COLLAR STRUCTURES USING A BEAM MODEL

Norwegian University of Science and Technology
13 July 2019

Sungsoo Lim

The Erasmus+: Erasmus Mundus MSc in Coastal and Marine Engineering and Management is an integrated programme including mobility organized by five European partner institutions, coordinated by Norwegian University of Science and Technology (NTNU).

The joint study programme of 120 ECTS credits (two years full-time) has been obtained at two or three of the five CoMEM partner institutions:

- Norges Teknisk- Naturvitenskapelige Universitet (NTNU) Trondheim, Norway
- Technische Universiteit (TU) Delft, The Netherlands
- Universitat Politècnica de Catalunya (UPC). BarcelonaTech. Barcelona, Spain
- University of Southampton, Southampton, Great Britain
- City University London, London, Great Britain

During the first three semesters of the programme, students study at two or three different universities depending on their track of study. In the fourth and final semester an MSc project and thesis has to be completed. The two-year CoMEM programme leads to a multiple set of officially recognized MSc diploma certificates. These will be issued by the universities that have been attended by the student. The transcripts issued with the MSc Diploma Certificate of each university include grades/marks and credits for each subject.

Information regarding the CoMEM programme can be obtained from the programme coordinator:

Øivind A. Arntsen, Dr.ing.
Associate professor in Marine Civil Engineering
Department of Civil and Environmental Engineering
NTNU Norway
Mob.: +4792650455 Fax: + 4773597021
Email: oivind.arntsen@ntnu.no

CoMEM URL: https://www.ntnu.edu/studies/mscomem

Disclaimer:
*"The European Commission support for the production of this publication does not constitute an endorsement of the contents which reflects the views only of the authors, and the Commission cannot be held responsible for any use which may be made of the information contained therein."*

# CoMEM Thesis

This thesis was completed by:
*Sungsoo Lim*

Under supervision of:
*PhD, Professor, Hans Bihs, Norwegian University of Science and Technology*
*PhD, Arun Kamath, Norwegian University of Science and Technology*
*PhD student, Tobias Martin, Norwegian University of Science and Technology*

As a requirement to attend the degree of
*Erasmus+: Erasmus Mundus Master in Coastal and Marine Engineering and Management (CoMEM)*

Taught at the following educational institutions:

*Norges Teknisk- Naturvitenskapelige Universitet (NTNU)*
*Trondheim, Norway*

*Technische Universiteit (TU) Delft*
*Delft, The Netherlands*

At which the student has studied from August 2017 to July 2019.

# Numerical Modelling for Fluid-Structure Interaction of Aquaculture Collar Structures using a Beam Model

A Thesis
submitted to the Faculty of Civil Engineering
at the Norwegian University of Science and Technology
in partial fulfillment of the requirements for the degree of

Master of Science

by

Sungsoo Lim

# Abstract

More and more aquaculture structures are installed in open water and further offshore due to the fact that a variety of conflicts have arisen with coastal water, eco-system, and inhabitants who live nearby. They can additionally benefit from a high energy environment, for example, strong currents and waves could disperse fish farm waste. However, an open water environment accompanies longer or steeper waves and harsher weather conditions where the structures could be exerted by a higher environmental loading and damaged by larger displacements or motions. Therefore, non-linear interaction between wave and structure needs to be investigated to get a better understanding of an accidental phenomenon which might impact on structures.

The collar structure above nets, shaped typically in a torus, consists of either single or double pipes, usually made of high-density polyethylene. Due to its slenderness and the material properties, the structure should be regarded as a flexible body and treated so in the structural analysis. In order to study its non-linearity, in addition, a coupling between structure and fluid surrounding the structure should be taken into account.

In this thesis, a 3-dimensional beam model is used for the collar structure and Newmark method is adopted for the time integration of structural dynamic analysis. To verify and validate a structure solver, which is developed in MATLAB, the results from the solver are examined with reliable sources including literatures and a commercial code, ANSYS Mechanical APDL 19.1. A free floating fluid model is established using an open-source CFD (Computational Fluid Dynamics) solver REEF3D. This fluid solver is capable of solving the Navier-Stokes equations for both water and air. With both solvers this thesis presents the numerical models and these set-ups as a good foundation to tackle nonlinear fluid-structure problem under the assumption the structures are flexible bodies. As a further step from the starting point this structural solver will be integrated into REEF3D to investigate fluid-structure interaction (FSI).

# Abstrakt

I denne oppgaven brukes en 3-dimensjonal strålemodell for fiske merd strukturen, og Newmark-metoden er vedtatt for tidintegrasjon av strukturell dynamisk analyse. For åverifisere og validere strukturløsningen utviklet i MATLAB sammenlignes resultater fra løsninger fra kjente kilder, som literatur og en kommersiell kode, ANSYS Mechanical APDL 19.1. En fri flytende modell er opprettet i den åpen kilde CFD (Computational Fluid Dynamics) modellen REEF3D. Modellen løser Navier-Stokes ligningene for både vann og luft. Med begge løsninger presenterer denne avhandlingen de numeriske modellene og disse oppsettene som et godt grunnlag for åtakle det ikke-lineære fluid-struktur problemet under antagelsen at strukturen er fleksibel. Som et ytterligere trinn fra utgangspunktet vil denne strukturelle løsningen bli integrert i REEF3D for åundersøke fluid-struktur-interaksjon (FSI).

# Acknowledgments

This thesis work is done to accomplish the requirement for a graduate student in the two years of Erasmus Mundus Master Course: Coastal and Marine Engineering and Management (CoMEM).

First, I would like to thank my main supervisor Hans Bihs for giving me the opportunity to be a part of this project. I would like to thank my co-supervisors Arun Kamath for his advice and guidance. Especially I thank to my co-supervisor Tobias Martin for his guidance and patience in dealing with all my questions during the time of this project. Also deeply appreciated is his assistance and the availability for discussions at all the time.

I would like to extend my gratitude to all my CoMEM class mates and my professor part of the CoMEM program within NTNU and TU Delft for the good times and support during the last two years. I especially thank Prof. Øivind Arnsten and Sonja Hammer, who particularly took care of the CoMEM cohort at NTNU. The last but not the less, I sincerely thank my wife, Jooyoung and my adorable Theo and Genie for their supports, who have made me the person I am. I thank them deeply for their unconditional love and constant motivation.

# Contents

# List of Figures

# List of Tables

# List of Symbols

| | |
|---|---|
| $a$ | wave amplitude |
| $A$ | cross section area of element |
| $c$ | speed of sound |
| $D$ | diameter of collar cross section |
| $E$ | Young's modulus or Elastic modulus |
| $f$ | nodal load |
| $\mathbf{F}$ | force (vector) |
| $g$ | gravitational acceleration |
| $G$ | shear modulus |
| $h$ | water depth |
| $H$ | wave height |
| $I$ | second moment of inertia |
| $IS$ | smoothness indicators |
| $J$ | torsional moment of inertia |
| $k$ | turbulent kinetic energy |
| $k$ | wave number |
| $\mathbf{K}$ | stiffness matrix |
| $L$ | length of element |
| $\mathbf{M}$ | mass matrix |
| $m$ | added mass |
| $n$ | the number of element |
| $P$ | point load |
| $p$ | pressure |
| $P_k$ | production rate |
| $PR$ | Poisson's ratio |
| $q$ | distributed load |
| $r$ | radius of gyration |
| $R$ | radius of collar cross section |
| $\mathbf{R}$ | rotation matrix |
| $t$ | time |

| | |
|---|---|
| $u$ | linear displacement components |
| $\mathbf{u}$ | displacement vector |
| $v$ | velocity |
| $V$ | volume |
| $w$ | vertical velocity |
| $w$ | (vertical) deflection |
| $\alpha, \beta, \gamma$ | angles between a local coordinate system and the global coordinate system in x, y, and z direction, respectively |
| $\alpha, \delta$ | trapezoidal parameters |
| $\Delta t$ | time step |
| $\Delta x$ | length of a cell side |
| $\epsilon$ | prestrain |
| $\tilde{\epsilon}$ | regularization parameter |
| $\eta$ | wave elevation |
| $\theta$ | angular displacement components |
| $\lambda$ | wave length |
| $\nu$ | kinematic viscosity |
| $\nu_t$ | eddy viscosity |
| $\rho$ | density |
| $\sigma_k$ | closure coefficient |
| $\Phi$ | shear deformation parameter |
| $\Phi$ | velocity potential |
| $\phi$ | level set function |
| $\omega$ | turbulent dissipation |
| $\omega$ | wave frequency |
| $\omega_0$ | natural frequency |

Superscripts

| | |
|---|---|
| $e$ | element |
| $[\ \ ]^T$ | matrix transpose |
| $[\ \ ]^{-1}$ | inverse matrix |
| $(\ \hat{}\ )$ | effective |
| $(\ \dot{}\ )$ | time derivative |
| $(\ \ddot{}\ )$ | second derivative with respect to time |

Subscripts

| | |
|---|---|
| $el$ | element (load) |
| $G$ | global coordinate system |
| $i, j$ | nodes |
| $L$ | local coordinate system |

| | |
|---|---|
| $n$ | node or nodal load |
| $w$ | water |
| $x, y, z$ | components of coordinates system |

# Chapter 1

# Introduction

## 1.1 Background

Traditional aquaculture industry has steadily managed lots of conflicts with natural and societal environments in coastal areas where the aquaculture structures would exploit those environments. For example, coastal water and ecosystem were degraded by wastes from fish farms. In addition, inhabitants have suffered from the degradation of their living environment due to disturbances in their neighbourhood.
A higher energy environment in open ocean is attractive to fish farmers. These natural environment conditions disperse the waste and ensure clear water. However, higher wave loading could affect fish cages because they are exposed a harsher weather condition which leads to larger motion or more severe damage to the structure.
According to a study conducted by Jensen[11], the structure failure is one of the major causes for fish escape. Considering the the aftermath of fish escape, eventually, the structure failure could escalate the severity of consequences up to the loss of investment, and the loss of reputation of operating companies.

In fact, there was a structure failure accident[1] in 2018 due to a winter storm in Nova Scotia, Canada, where a total structural failure occurred. The parts of the cage were torn and drifted to the coast. The most severe loss was that all the fishes were escaped and the operating company was fined.

### 1.1.1 Aquaculture structure

Aquaculture structures where fishes grow are called by net pens or fish cages. The shape of the structure is basically either rectangular or circular. A circular or a torus-

[1]Source: https://responsibleaquaculture.wordpress.com

Figure 1.1: An example of structure failure

shaped fish cage is made of high-density Polyethylene (HDPE) while the rectangular cage is usually of steel material.[3]
The figure below shows a schematic drawing of a typical aquaculture structure.

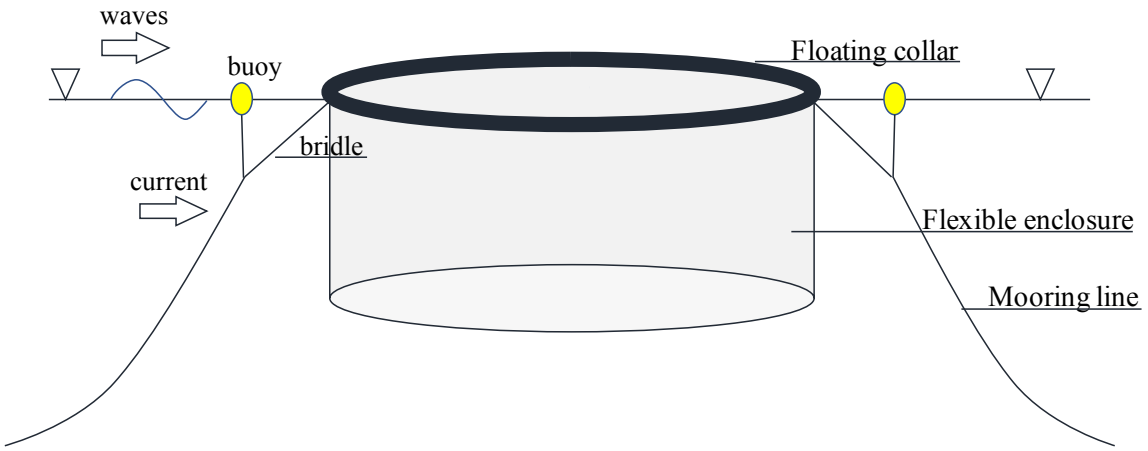


Figure 1.2: A simplified model of aquaculture structure

Floating collars provide the necessary buoyancy such that the whole structure swims. Net structures beneath the collars are permeable. Thus water can freely inflow from outside and flooded out from the structure inside again. Mooring lines are attached to the floating collar. The mooring lines prevent the whole structure being drifted away from the original location and withstand the loads from the environment by utilising its tensioning capability and rigidity.

Since the most of the structural parts have basically positive buoyancy, a heavy weight - for instance, the weight inside sinker pipes in Figure 1.3 - should be in place to stabilise the whole structure. The inertia bears vertical load and by the gravity the

external energy is dissipated into the motion of the structure. This energy is eventually transferred to wave-making energy by the motion of the structures. Mooring lines primarily withstand the horizontal load from waves and currents.

### 1.1.2 Collar structure

Floating collars are pipe-looking structures or a group of these structures in case the structures are made of plastic, i.e. HDPE, connected to net and mooring line, as shown in Figure 1.3.[2]

Not to mention its material properties, the slenderness of a collar structure lets

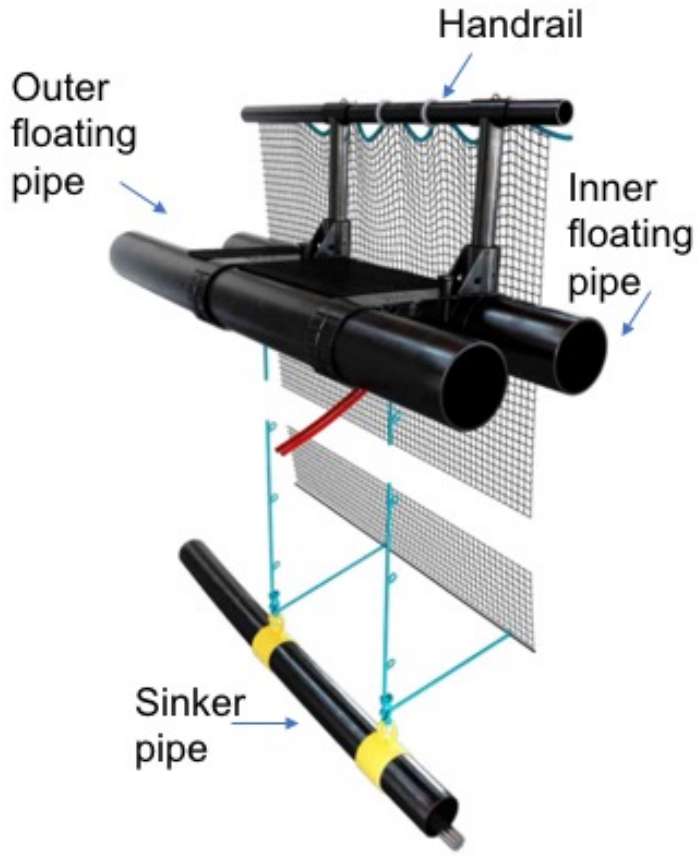


Figure 1.3: The configuration of typical aquaculture structures floating collar

analysers regard the structure as a flexible body when large motions or displacements of the structure are examined since the structure becomes very subject to bending failure. Thus, shear stress might be rather less important attributed to relatively

[2]Source: https://www.akvagroup.com/pen-based-aquaculture/pens-nets/plastic-pens

small cross section areas due to its slenderness, whereas most of the deflections can be contributed by bending stress. The chapter 2 will deal with this.

### 1.1.3 Environmental load

The site condition for open water fish farms is relatively rough compared to the place in which the aquaculture structures commonly used to be located onshore or nearshore. Therefore, the aquaculture structures in open water should withstand harsher environmental load without mitigation measures due to its difficulty of human intervention such as disconnecting and sheltering, of which a means of mitigation is taken against accidental events in other industries such as oil and gas industry. Thus, this higher environmental loading is inevitable.

## 1.2 Failure Modes

A failure of aquaculture structure can be defined by any accidental event resulting in a loss of people, investment, or reputation of operating companies. In most cases, the structure itself is operated without residential supervision by human. Thus, the fatalities due to the failure is very remote. Nonetheless, loss of investment or reputation could be caused by a significant structure failure or by an accidental fish escape. Therefore, the followings are possible examples of failure modes of aquaculture structures induced by interactions between structures and surrounding fluid.

- **Direct damage to piping**
  A rougher wave or current load could concentrate a small part of the structure and it could damage the part resulting in a puncture or a buckling of the structure due to the excessive bending moment or shear stress. The root cause of this damage is not easily defined and identified that is why fluid-structure interaction need to be investigated.

- **Wave overtopping**
  Literally water can go beyond the floating collar, in terms of vertical displacement. Hydrostatic or -dynamic pressure will instantaneously soar and lead to structural deformation so the relation between fluid and structure should be examined.

- **Submergence induced by current drag** [3]
  When a cage is subjected to a current, the net will generate a drag force that will be loaded on the mooring system. The buoys of the mooring system are subjected to a resulting downward pull generated by the cumulative effect of loads on the bridle - floater to buoy (See Figure 1.2) - and mooring line. This

downward load is contrasted with the upward buoyancy. If the buoys are too small, buoyancy will be less than the downward load, and the buoy and the cage collar will become submerged in strong current conditions.

- **Net integrity failure**
  There are a number of reasons to cause net integrity failure, for example, excessive shear stress, predator bite, caged fish bite, rope knotting failure.[3] This means a penetration through the net, which allows fish to escape.

Some of these failures or resultant damages cannot be handled by a simple engineering tool and theory especially when the consequences of the accidental events should be investigated in a precise way. For example, non-linear wave structure interaction could play a role in some failure modes including direct damage and wave overtopping amongst those of the mentioned above.

## 1.3 State of the Arts

There is a limited number of literature that has dealt with dynamic behaviour of aquaculture collar structure while considering the non-linearity from the resultant behaviour of the structure by the exerted forces and stresses.

Huang, Tang and Liu [10] analysed net and mooring lines as a flexible body using a lumped mass method but did not consider collar structures. Xu et al.[24] carried out physical experiment and numerical analysis. They used a torus collar model with linear wave but they did not study any interaction between fluid and structure.
Kristiansen and Faltinsen [17], studied both numerical analysis and physical experiment. In addition, they used a more sophisticated model including collar, net, and mooring line. They found a significant load increase due to wave overtopping in longer and steeper wave. They introduced a modal theory to represent bending stiffness and hydrodynamic nonlinearity. But, they did not directly use flexible body analysis.
Fredriksson and Tsukrov[21] [7] [6] constructed a methodical numerical modelling which incorporated the finite element method (FEM), particularly, the equivalent truss method solved by a Newmark method. Regarding the environmental load, they used a wave spectrum representing a storm case and employed the Morrison equation for hydrodynamic forces to apply on the elements. Instead of using CFD, they applied hydrodynamic coefficient for the equation of motions and Morrison's equation for hydrodynamic force calculations.

## 1.4 Objectives

In this thesis, the idea of using flexible body in a numerical model will be examined and validated with reliable sources. It is suggested under the circumstances where diverse failure mechanisms would drive structural failure, particularly induced by nonlinear wave actions. The idea itself is not supported by using either a rigid body analysis or the potential theory or a combination of them. Thus, a beam model using the finite element method is dedicatedly constructed which can be integrated into a Computational Fluid Dynamics (CFD). This could give an insight from a different perspective than existing studies while pinpointing the nonlinear interaction between fluid and structure.

The objectives of this thesis is to build the basis for modelling the fluid-structure interaction between aquaculture collar structure and the surrounding fluid in waves and currents by using a finite element (FE) model for the collar and the open source CFD code, REEF3D, for solving the surrounding fluid. For this purpose, some of input parameters and their effects can be assumed to be negligible in case they do not play a significant role in achieving this objective.

There might be a question about the development of a new code since several open library of finite element method exist. The thesis work is, however, a part of an ambitious project where the application could extend to higher order scheme computation to accommodate other structural models and to construct whole aquaculture structure models eventually.

## 1.5 Terminology

Common terminologies within the thesis are summarised below:

- **Accuracy**
  The level of closeness or agreement to the exact (analytic) solution for a numerical scheme. In order for a numerical scheme to be accurate, the scheme simply should not introduce numerical damping too much. In this sense, higher-order methods are generally less stable but more accurate. Thus, an appropriate balance between stability and accuracy needs to be found.

- **Integration error**
  For structural analysis, Bathe [1] defined the errors in integration can be measured in terms of period elongation and amplitude decay compared to the exact solution. In this thesis, therefore, a phase error is defined by the average period elongation among multiple oscillations in a transient solution and the amplitude

error is defined by maximum amplitude decay among these oscillations. When these errors are presented by percentage, the error-to-reference value ratio is used where the reference value is the exact solution and the error is presented in the absolute value.

- **Consistency**
  A relation between a numerical scheme and a differential equation. The numerical scheme is consistent if the error converges to zero as $\Delta t \to 0$.

- **Convergence**
  The solution of the numerical scheme converges towards the exact solution of a differential equation for $\Delta t, \Delta x \to 0$.

- **Stability**
  A stable method should not diverge over time. For example, an error caused by a small perturbation in the numerical solution would not be regarded as unstable.

# Chapter 2

# Numerical model

As addressed in Chapter 1, this thesis deals with the subjects concerned structural problems and interactions with surrounding fluid. Some of these problems and damages cannot be handled by a popular engineering method and tool such as potential theory and rigid body analysis, which is relatively simple to follow. Due to the limitation of the compatibility of these methods and tools, however, CFD and finite element analysis are used in this thesis to tackle those problems that include atypical characteristics such as nonlinear interaction.

## 2.1 Structural Model

A structural model eventually will be solved using the equation of motions for 3-dimensional ("3-D") beam model. The following features and those explanations will comprise a structural solver and determine the capability of the solver.

### 2.1.1 Governing equation

A floating collar is modelled by a flexible body composed of by a finite number of elements. Consulting ANSYS BEAM object definitions [16] [25], both bending and shear stress are importantly considered in a beam model. Both elongation and torsion are considered with respect to the axis of the beam model. "BEAM" specifically stands for a type of ANSYS object, whereas the model developed to analyse here is called by "beam" model.
The governing equation for dynamic behaviour for the beam model is identical to an equation of motion for a mass-spring system.
The structural solver that this Chapter explains will solve this following equation:

$$\left[\mathbf{M}\right]\ddot{\mathbf{u}}(t) + \left[\mathbf{K}\right]\mathbf{u}(t) = \mathbf{F}(t) \tag{2.1}$$

Where, **K** is a stiffness matrix and **M** is a mass matrix. **u**(t) is a displacement vector as a function of time and **F**(t) is a time-varying force vector. The dimensions of matrices and vectors are determined by the number of elements and the dimension of the beam model, e.g. 2-D or 3-D.

In the governing equation of the thesis, Equation 2.1, a hydrodynamic damping term is neglected at this moment for the simplification of the model. If required, the damping term can be determined by hydrodynamic damping coefficients with respect to the six degree of freedoms e.g. surge, sway, heave, roll, pitch, and yaw, generally obtained by free-decaying tests.

#### 2.1.1.1 Displacement vector

The 3-dimensional beam has six degree of freedom per node. Thus, a single element has twelve degrees of freedom in total. That is why 12 components are assigned for a displacement vector in Equation 2.2, where each $n$-th component of the displacement vector denotes each numbered axis in a local coordinate system as shown in Figure 2.1. Either columns or rows of the matrix **K** or **M** for one element follow the same numbering in terms of the order of components with those of Figure 2.1.
In short, the numbers in the Figure 2.1 stand for the $n$-th components in an element

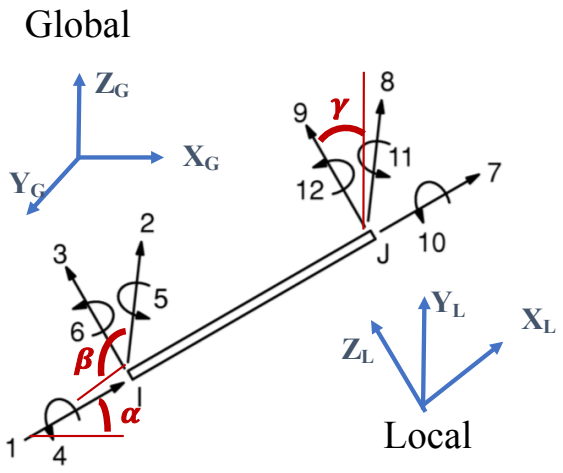


Figure 2.1: The local and global coordinate system for an element

displacement with respect to the local coordinate system. The superscript $e$ in Equation 2.2 means "element" so each element has its own displacement vector. Thus, the

rotation matrix is introduced to transform from the orientation of the local coordinate system to the orientation of the global coordinate system as shown in Equation 2.3. Here, the rotation is made by such a linear operator so the rotation preserves the origin of the rotation. In other words, the magnitudes of the position vectors are preserved even after they have been transformed.

$$\mathbf{u^e} = \begin{Bmatrix} u_{xi} \\ u_{zi} \\ u_{yi} \\ \theta_{xi} \\ \theta_{yi} \\ \theta_{zi} \\ u_{xj} \\ u_{yj} \\ u_{zj} \\ \theta_{xj} \\ \theta_{zj} \\ \theta_{yj} \end{Bmatrix} \begin{matrix} \longrightarrow \text{linear displacement in x direction for node i} \\ \longrightarrow \text{linear displacement in z direction for node i} \\ \longrightarrow \text{linear displacement in y direction for node i} \\ \longrightarrow \text{angular displacement (torsion) for node i} \\ \longrightarrow \text{angular displacement in z direction for node i} \\ \longrightarrow \text{angular displacement in y direction for node i} \\ \longrightarrow \text{linear displacement in x direction for node j} \\ \longrightarrow \text{linear displacement in z direction for node j} \\ \longrightarrow \text{linear displacement in y direction for node j} \\ \longrightarrow \text{angular displacement (torsion) for node j} \\ \longrightarrow \text{angular displacement in z direction for node j} \\ \longrightarrow \text{angular displacement in y direction for node j} \end{matrix} \tag{2.2}$$

In this particular case, the local coordinate makes use of right-handed coordinate system while the global coordinate employs the left-handed coordinates. Indeed, it has nothing to do with final results no matter which coordinate system is chosen. Here as shown in Figure 2.1 the angles $\alpha$,$\beta$, and $\gamma$ stand for angles between a local coordinate system and the global coordinate system in $x$, $y$, and $z$ direction, respectively.

$$\begin{aligned} \mathbf{R_Z R_Y R_X} &= \begin{pmatrix} cos\gamma & -sin\gamma & 0 \\ sin\gamma & cos\gamma & 0 \\ 0 & 0 & 1 \end{pmatrix} \begin{pmatrix} cos\beta & 0 & sin\beta \\ 0 & 1 & 0 \\ -sin\beta & 0 & cos\beta \end{pmatrix} \begin{pmatrix} 1 & 0 & 0 \\ 0 & cos\alpha & -sin\alpha \\ 0 & sin\alpha & cos\alpha \end{pmatrix} \\ &= \begin{pmatrix} cos\gamma cos\beta & -sin\gamma cos\alpha + cos\gamma sin\beta sin\alpha & sin\gamma sin\alpha + cos\gamma sin\beta cos\alpha \\ sin\gamma cos\beta & cos\gamma cos\alpha + sin\gamma sin\beta sin\alpha & -cos\gamma sin\alpha + sin\gamma sin\beta cos\alpha \\ -sin\beta & cos\beta sin\alpha & cos\beta cos\alpha \end{pmatrix} \end{aligned} \tag{2.3}$$

#### 2.1.1.2 Mass matrix

According to a ANSYS document [16] and Yokoyama [25], a mass matrix for one element is constituted up by the components below:

$$\left[M_L\right] = M_t \begin{bmatrix} 1/3 & & & & & & & & & & & \\ 0 & A_z & & & & & & & & & & \\ 0 & 0 & A_y & & & & & & \text{Symmetric} & & & \\ 0 & 0 & 0 & J_x/3A & & & & & & & & \\ 0 & 0 & -C_y & 0 & E_y & & & & & & & \\ 0 & C_z & 0 & 0 & 0 & E_z & & & & & & \\ 1/6 & 0 & 0 & 0 & 0 & 0 & 1/3 & & & & & \\ 0 & B_z & 0 & 0 & 0 & D_z & 0 & A_z & & & & \\ 0 & 0 & B_y & 0 & -D_y & 0 & 0 & 0 & A_y & & & \\ 0 & 0 & 0 & J_x/6A & 0 & 0 & 0 & 0 & 0 & J_x/3A & & \\ 0 & 0 & D_y & 0 & F_y & 0 & 0 & 0 & C_y & 0 & E_y & \\ 0 & -D_z & 0 & 0 & 0 & F_z & 0 & -C_z & 0 & 0 & 0 & E_z \end{bmatrix} \tag{2.4}$$

where, $M_t = (\rho A + m)L(1-\epsilon)$ $[kg]$,
$A$ = cross-section area of element $[m^2]$, $L$ = the length of element $[m]$
$\rho$ = the density of element material $[kg/m^3]$
$m$ = added mass per unit length $[kg/m]$, $\epsilon$ = prestrain $[-]$

Here, the added mass, $m$, and the prestrain, $\epsilon$, were assumed to be zero for the purpose of this thesis described in Section 1.4.

$$A(r,\Phi) = \frac{\frac{13}{35}+\frac{7}{10}\Phi+\frac{1}{3}\Phi^2+\frac{6}{5}(r/L)^2}{(1+\Phi)^2}$$

$$B(r,\Phi) = \frac{\frac{9}{70}+\frac{3}{10}\Phi+\frac{1}{6}\Phi^2-\frac{6}{5}(r/L)^2}{(1+\Phi)^2}$$

$$C(r,\Phi) = \frac{(\frac{11}{210}+\frac{11}{120}\Phi+\frac{1}{24}\Phi^2+(\frac{1}{10}-\frac{1}{2}\Phi)(r/L)^2)L}{(1+\Phi)^2}$$

$$D(r,\Phi) = \frac{(\frac{13}{420}+\frac{3}{40}\Phi+\frac{1}{24}\Phi^2-(\frac{1}{10}-\frac{1}{2}\Phi)(r/L)^2)L}{(1+\Phi)^2}$$

$$E(r,\Phi) = \frac{(\frac{1}{105}+\frac{1}{60}\Phi+\frac{1}{120}\Phi^2+(\frac{2}{15}+\frac{1}{6}\Phi+\frac{1}{3}\Phi^2)(r/L)^2)L^2}{(1+\Phi)^2}$$

$$F(r,\Phi) = \frac{-(\frac{1}{140}+\frac{1}{60}\Phi+\frac{1}{120}\Phi^2+(\frac{1}{30}+\frac{1}{6}\Phi-\frac{1}{6}\Phi^2)(r/L)^2)L^2}{(1+\Phi)^2}$$

$$A_z = A(r_z,\Phi_y) \qquad A_y = A(r_y,\Phi_z)$$
$$B_z = B(r_z,\Phi_y) \qquad B_y = B(r_y,\Phi_z)$$
$$\ldots$$
$$F_z = F(r_z,\Phi_y) \qquad F_y = F(r_y,\Phi_z)$$

$$\Phi_y = \frac{12EI_z}{GA_zL^2}[-] \qquad \Phi_z = \frac{12EI_y}{GA_yL^2}[-]$$

where, $\Phi$ : Shear deformation parameter [25],

$r_y = \sqrt{\frac{I_{yy}}{A}}[m]$ : radius of gyration with reference to y-axis of a cross section in case of a beam
$r_z = \sqrt{\frac{I_{zz}}{A}}[m]$ : radius of gyration with reference to z-axis of a cross section in case of a beam

#### 2.1.1.3 Stiffness matrix

A stiffness matrix, **K**, whereas, is composed of the following components.

$$\left[K_L\right] = \begin{bmatrix} AE/L & & & & & & & & & & & \\ 0 & a_z & & & & & & & & & & \\ 0 & 0 & a_y & & & & & & \text{Symmetric} & & & \\ 0 & 0 & 0 & GJ/L & & & & & & & & \\ 0 & 0 & d_y & 0 & e_y & & & & & & & \\ 0 & c_z & 0 & 0 & 0 & e_z & & & & & & \\ -AE/L & 0 & 0 & 0 & 0 & 0 & AE/L & & & & & \\ 0 & b_z & 0 & 0 & 0 & d_z & 0 & a_z & & & & \\ 0 & 0 & b_y & 0 & c_y & 0 & 0 & 0 & a_y & & & \\ 0 & 0 & 0 & -GJ/L & 0 & 0 & 0 & 0 & 0 & GJ/L & & \\ 0 & 0 & d_y & 0 & f_y & 0 & 0 & 0 & c_y & 0 & e_y & \\ 0 & c_z & 0 & 0 & 0 & f_z & 0 & d_z & 0 & 0 & 0 & e_z \end{bmatrix} \tag{2.5}$$

where, E = Young's modulus $[N/m^2]$,
G = Shear modulus = $\frac{E}{2(1+PR)}$ $[N/m^2]$,
PR = Poisson's ratio [-],
J = torsional moment of inertia = $\begin{pmatrix} J_x \text{ if } I_x = 0 \\ I_x \text{ if } I_x \neq 0 \end{pmatrix}[m^4]$

$a_y = a(I_y, \Phi_z)$,
$b_z = b(I_z, \Phi_y)$,
...
$f_y = f(I_y, \Phi_z)$,
$f_z = f(I_z, \Phi_y)$,

and where,
$a(I,\Phi) = \frac{12EI}{L^3(1+\Phi)}$ $\quad b(I,\Phi) = -\frac{12EI}{L^3(1+\Phi)}$ $\quad c(I,\Phi) = \frac{6EI}{L^2(1+\Phi)}$
$d(I,\Phi) = -\frac{6EI}{L^2(1+\Phi)}$ $\quad e(I,\Phi) = \frac{(4+\Phi)EI}{L(1+\Phi)}$ $\quad f(I,\Phi) = \frac{(2-\Phi)EI}{L(1+\Phi)}$

$\Phi_y = \frac{12EI_z}{GA_zL^2}[-]$ $\quad \Phi_z = \frac{12EI_y}{GA_yL^2}[-]$

In case the number of elements is extremely small, the shear deformation parameter $\Phi \to 0$, since $GAL^2 \gg 12EI$ , $\Phi_y$ and $\Phi_z \to 0$. Here is the example calculation if the collar is modelled of either steel or HDPE, where the floater pipe diameter is

Table 2.1: Material properties for steel and HDPE

| | unit | Steel | HDPE |
|---|---|---|---|
| $G$ | $Pa = N/m^2$ | $7.692e+10$ | $6.897e+7$ |
| $PR$ | - | 0.3 | 0.45 |
| $E$ | $Pa = N/m^2$ | $2e+11$ | $2e+8$ |

Table 2.2: $\Phi$ value with respect to the number of element (Total Length = 180 $m$)

| | n=30 | | n=60 | | n=90 | |
|---|---|---|---|---|---|---|
| | Steel | HDPE | Steel | HDPE | Steel | HDPE |
| $L[m]$ | 6 | 6 | 3 | 3 | 2 | 2 |
| $\Phi$ | 2.41e-02 | 2.68e-02 | 9.62e-02 | 1.0e-01 | 2.16e-01 | 2.41e-01 |

assumed to 0.5 m and the thickness of the pipe is 30 mm. Assuming that the total length of the structure to be calculated is 180 m, and the number of elements can vary with 30, 60, and 90.

As the length of an element decreases and the number of elements increases, e.g. 2 $m$ and $n$= 90, however, $\Phi$ value is way greater than those of longer element lengths' cases. Thus, the shear deformation cannot be disregarded in this application.

An application case in the thesis requires at least 30 elements considering the representation of torus shape. Accordingly, $\Phi$ parameter is around 2.7 % in case the number of element is 30. As the number of element increases e.g. 90, a gravity effect would play a role in deformations since shear deformations account for a significant portion of total deformations.[25]

#### 2.1.1.4 Force vector

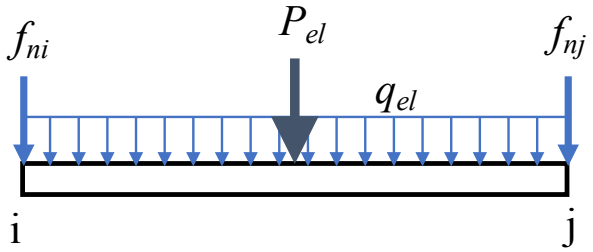


Figure 2.2: Element forces and nodal forces under vertical loading

Force vectors, $F$, are calculated by a shape function as described below for relevant component to a vertical load. The vectors superpose the multiple loads such as nodal loads, $f_n$, element point loads, $P_{el}$ and element distributed loads, $q_{el}$, and transform eventually into equivalent nodal loads in both ends (nodes). In order to do so, each summation over the equivalent nodal loads is applied for respective corresponding components. Equation 2.6 shows an example in case of a combination of multiple vertical loads are only applied.

$$\{F_L\} = \left\{ \underbrace{P_{el} + q_{el}}_{\text{element force}} + \underbrace{f_n}_{\text{nodal force}} \right\} = \begin{Bmatrix} 0 \\ \frac{P}{2} \\ 0 \\ 0 \\ 0 \\ -\frac{PL^2}{8} \\ 0 \\ \frac{P}{2} \\ 0 \\ 0 \\ 0 \\ \frac{PL^2}{8} \end{Bmatrix} + \begin{Bmatrix} 0 \\ \frac{1}{2}qL \\ 0 \\ 0 \\ 0 \\ -\frac{1}{12}qL^2 \\ 0 \\ \frac{1}{2}qL \\ 0 \\ 0 \\ 0 \\ \frac{1}{12}qL^2 \end{Bmatrix} + \begin{Bmatrix} 0 \\ f_{ni} \\ 0 \\ 0 \\ 0 \\ 0 \\ 0 \\ f_{nj} \\ 0 \\ 0 \\ 0 \\ 0 \end{Bmatrix} \tag{2.6}$$

where, $q_{el}$ is an evenly distributed load along an element, $P_{el}$ means a point load applying on midspan of the element. $f_n$ is a point load exerting on a node. The reason why only 2nd, 6th, 8th and 12th components are non-zero is that only vertical components ($z-$ direction in local coordinate) of the load are applied here. If there are horizontal ($x-$ direction in local coordinate) or lateral ($y-$ direction in local coordinate) components for an applying load, other vector components should be non-zero by the definition of the force vector.

The terminology "force" is commonly used for both external force and internal force in structural analysis. Still, the forces mean external forces, which is simultaneously called "load" in this matter. In the thesis, hydrodynamic loading can be discretized by a form of element point load and then transformed into equivalent nodal load for matrix calculations.

#### 2.1.1.5 Assembling of matrices

To solve the equation of motion, transformations in a global coordinate system are prerequisite due to that there are finite number of respective local coordinate systems co-exist. Accordingly, it is compulsory to assemble **M** and **K** matrices into the global

coordinate. It enables analysers to calculate finite number of elements at a time by inverting matrices in static analyses and by numerical integration in dynamic analyses.
While the element-wise matrices are assembled, the components for the same node from different matrices are summated by superposition. Thus, Figure 2.3, where the overlapped areas in matrices mean summations over the components from different element-wise matrices, illustrates how the assembled matrix looks if elements are linked up either in a way of being unclosed or enclosed.

Once the equation is solved, one will find the result value in a form of global displacement vector which can be decomposed by a finite number of element-wise displacement vectors. The dimension of the global displacement vector is determined by the total degree of freedom of the corresponding numerical model. As illustrated in Figure 2.3, an enclosed type of beam model has less degree of freedom in total than an unclosed types of beam model does. That is because the first element and the last element have been coupled in the former during assembling the **M** and **K** matrices. Here in the thesis, an enclosed type of beam has been used.

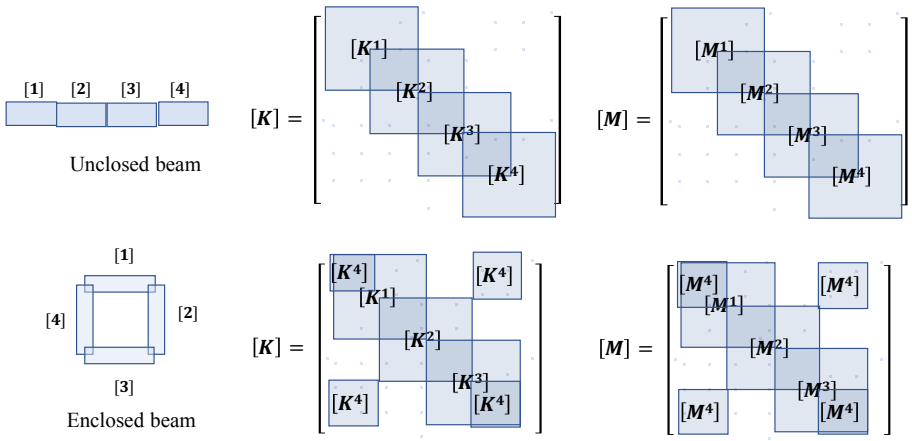


Figure 2.3: Assembling of M and K element-wise matrices

### 2.1.2 Material properties

A beam model imitating collar structures has been assumed to have a torus or a ring shape on overall and a circular cross-section. In fact, the cross-section of the beam mostly has a hollow part inside, like a cross-section of a pipe. According to a report for aquaculture structure manufacturing [3], some of pipes can be filled with polystyrene inside to ensure that the cage afloat even if the pipes become damaged and flooded. In the numerical model, this high reserve buoyancy is not modelled

for the simplicity. Instead, a hollow section inside - a very low density - has been compensated with an effective material density of the total volume. A pipe element is assumed to be submerged by the radius of its outer circle of cross section as shown in Figure 2.4 because other parts of aquaculture structure have not been involved in the numerical model. e.g. net, mooring lines, or handrails. That is the reason why the effective density has been introduced for the material density.

However, this does not mean the density of floating structure requested by REEF3D should be identical to this effective density. That is because the effective density is introduced to reflect the state of being afloat and the thickness of the material which determine the moment of inertia of the cross section resulting in the corresponding stiffness. Consequently, the applicable densities of the material should be different in two solvers since the fluid solver does not take the thickness of the element into account. The effective density can be derived as the submerged volume is assumed

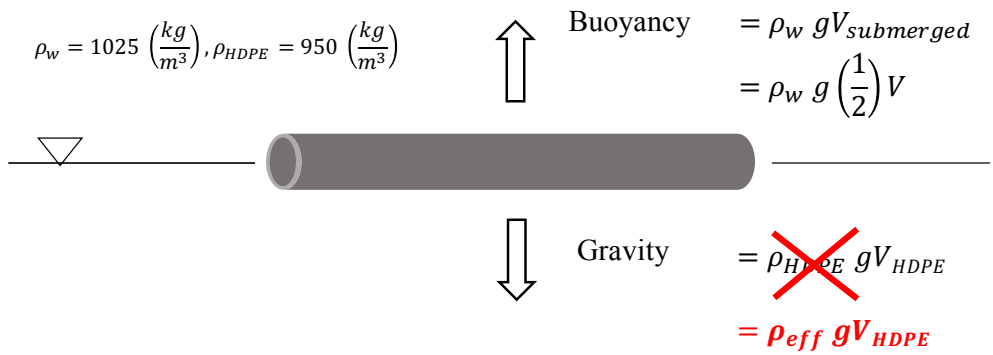


Figure 2.4: Effective density

to be a half of the intact cylinder volume with a outer diameter:

$$\rho_{eff} = \rho_w \frac{V}{2V_{HDPE}} = \rho_w \frac{\pi R_o^2 L}{2\pi(R_o^2 - R_i^2)L} = \frac{\rho_w R_o^2}{2(R_o^2 - R_i^2)} \tag{2.7}$$

Where, $R_o$: outer radius, $R_i$: inner radius, $V$: intact cylinder volume, $V_{HDPE}$: HDPE pipe volume, $V_{submerged}$ : Submerged volume = a halved intact cylinder volume

### 2.1.3 Meshing

There are three meshing processes during the entire analysis of the thesis work. First one is required to solve the structural analysis i.e. finite element analysis. Thus, each element can be regarded as a mesh here, where the mesh is cut perpendicular to the longitudinal axis of the beam like BEAM object is in ANSYS, specifically BEAM3 or

BEAM4 objects, as illustrated in Figure 2.5. This mesh is rather called by “element” not to confuse with other mesh processes.

Secondly, a meshing is required to transfer data to fluid solver. A STL (stereolithog-

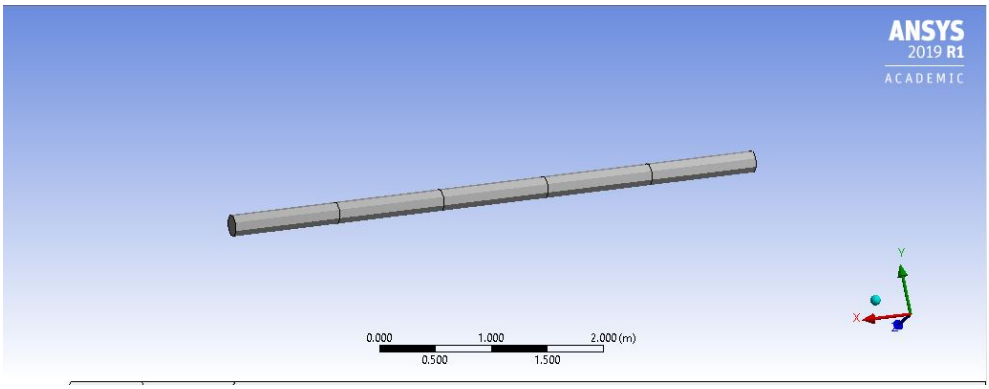


Figure 2.5: ANSYS BEAM Object and meshes i.e. 5 elements

raphy) file format is used for this data exchange and a triangular type of mesh is needed here, constituting a surface. Figure 2.6 shows a plot from a STL format that is used in the meshing process.

Lastly, the fluid solver requires a meshing of calculation domain as well. The follow-

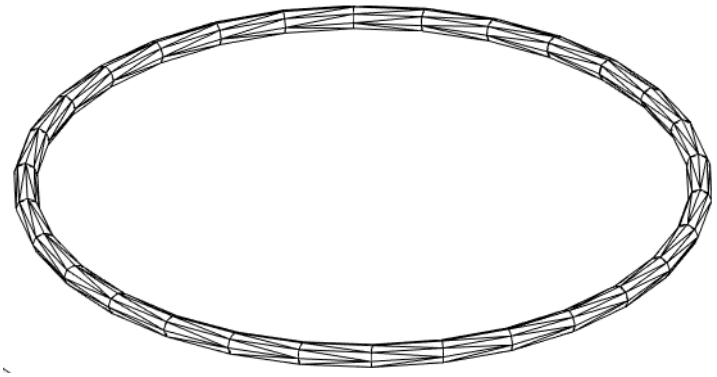

Figure 2.6: A STL format output and triangular meshes

ing chapter will handle this.

### 2.1.4 Boundary condition

There is no fixed point vertically in a floating collar model when the vertical loads only apply. In case horizontal or lateral load apply e.g. current load, however, a fixed point should be defined in order to prevent the model being drifted.

### 2.1.5 Time integration : Newmark Method

For the time integration of the numerical computation to solve the dynamic beam equation, the Newmark method is adopted for the structural solver. The method is introduced by Newmark in 1959.[1] Newmark method is one of proper numerical schemes for the purpose of thesis in that the scheme is second order, popular in fluid-structure interaction. [1] Above all, it is an implicit method in that the scheme is always stable regardless of time step sizing. Newmark was originally proposed the scheme as an unconditionally stable scheme, where $\delta = \frac{1}{2}$, $\alpha = \frac{1}{4}$ as shown in Equation 2.8. However, the scheme can have unstable condition if it employs different trapezoidal parameters of $\delta$ and $\alpha$.
To be noted here is that any numerical solution has its own accuracy whether it is implicit or explicit. That is why a thorough preparation should be implemented for setting input parameters, e.g. time step, corresponding a numerical scheme. Regarding a higher accuracy in general, the following Section 2.1.5.3 will explain more.[1]

#### 2.1.5.1 Definition

From Bathe's definition [1], the numerical scheme can be described by the objective where one needs to find the acceleration vector for a new time step. Thus, a kinds of numerical technique is required to deal with this because the scheme is implicit so still there are unknown arguments in the right hand side in Equations 2.8, e.g. $\ddot{U}_{t+\Delta t}$. That is the reason why so-called "effective stiffness matrix" and "effective load" should be introduced. Therefore, the new displacement can be found first and then the new acceleration can be evaluated later on.

$$\begin{aligned} \dot{\mathbf{u}}_{t+\Delta t} &= \dot{\mathbf{u}}_t + [\delta \ddot{\mathbf{u}}_{t+\Delta t} + (1-\delta)\ddot{\mathbf{u}}_t]\Delta t \\ \mathbf{u}_{t+\Delta t} &= \mathbf{u}_t + \dot{\mathbf{u}}_t \Delta t + [\alpha \ddot{\mathbf{u}}_{t+\Delta t} + (\frac{1}{2} - \alpha)\ddot{\mathbf{u}}_t]\Delta t^2 \end{aligned} \tag{2.8}$$

Where, the trapezoidal parameters, $\delta = \frac{1}{2}$ and $\alpha = \frac{1}{4}$.

#### 2.1.5.2 Application

To construct this method in a practical computation, integration constants should be introduced:

$$\begin{aligned} a_0 &= \frac{1}{\alpha \Delta t^2}; \quad a_1 = \frac{\delta}{\alpha \Delta t}; \quad a_2 = \frac{1}{\alpha \Delta t}; \quad a_3 = \frac{1}{2\alpha} - 1; \\ a_4 &= \frac{\delta}{\alpha} - 1; \quad a_5 = \frac{\Delta t}{2}(\frac{\delta}{\alpha} - 2); \quad a_6 = \Delta t(1-\delta); \quad a_7 = \delta \Delta t; \end{aligned} \tag{2.9}$$

The effective stiffness matrix can be derived as:

$$\hat{\mathbf{K}} = \mathbf{K} + a_0\mathbf{M} \tag{2.10}$$

Where, stiffness matrix $\mathbf{K}$ and mass matrix $\mathbf{M}$. And, the effective loads at time $t+\Delta t$ can be calculated by:

$$\hat{\mathbf{F}}_{t+\Delta t} = \mathbf{F}_{t+\Delta t} + \mathbf{M}(a_0\mathbf{u}_t + a_2\dot{\mathbf{u}}_t + a_3\ddot{\mathbf{u}}_t) \tag{2.11}$$

Solving for displacement at the new time, $t + \Delta t$,

$$\mathbf{u}_{t+\Delta t} = \hat{\mathbf{K}}^{-1}\hat{\mathbf{F}}_{t+\Delta t} \tag{2.12}$$

Accordingly, accelerations and velocities at time $t + \Delta t$ can be calculated by:

$$\ddot{\mathbf{u}}_{t+\Delta t} = a_0(\mathbf{u}_{t+\Delta t} - \mathbf{u}_t) - a_2\dot{\mathbf{u}}_t - a_3\ddot{\mathbf{u}}_t \tag{2.13a}$$

$$\dot{\mathbf{u}}_{t+\Delta t} = \dot{\mathbf{u}}_t + a_6\ddot{\mathbf{u}}_t + a_7\ddot{\mathbf{u}}_{t+\Delta t} \tag{2.13b}$$

#### 2.1.5.3 Time step

The Newmark scheme is implicit that is why the scheme has no restriction on the time step size, however, the schemes is not always accurate compared to exact solution as mentioned above. According to Bathe [1], while using an unconditionally stable operator like the Newmark method, the time step has to be chosen to yield an accurate and effective solution. According to Bathe[1] and Kleiven [15], it is generally suggested that a required time step for each element is dependent on the stiffness, in terms of elastic modulus ($E$), the characteristic length ($L$), and the density of each element. Here, the time step implies the time it takes for the sound to pass the smallest element (or element side) in the model. However, this time step cannot be regarded as an crucial requirement in this thesis but considered as a reference.

$$\Delta t < \frac{L}{c} \tag{2.14}$$

where, $c^2 = \frac{E}{\rho}$ and the characteristic length, L= length of the smallest beam element in case of beam object. Apperently, $c$= the speed of sound in a material.

Wiebe and Stanciulescu [23] studied inconsistent stability of Newmark's method in structural dynamics applications, where the method implies Newmark family. The term "family" accounts for more general expression of the scheme, in which $\delta$ and $\alpha$ can vary in some applications. In order to check the stability of these applications, the approximate time step check can be used. e.g. $\Delta t < \sqrt{-1/\omega_0^2\alpha}$ , where $\omega_0^2$ is

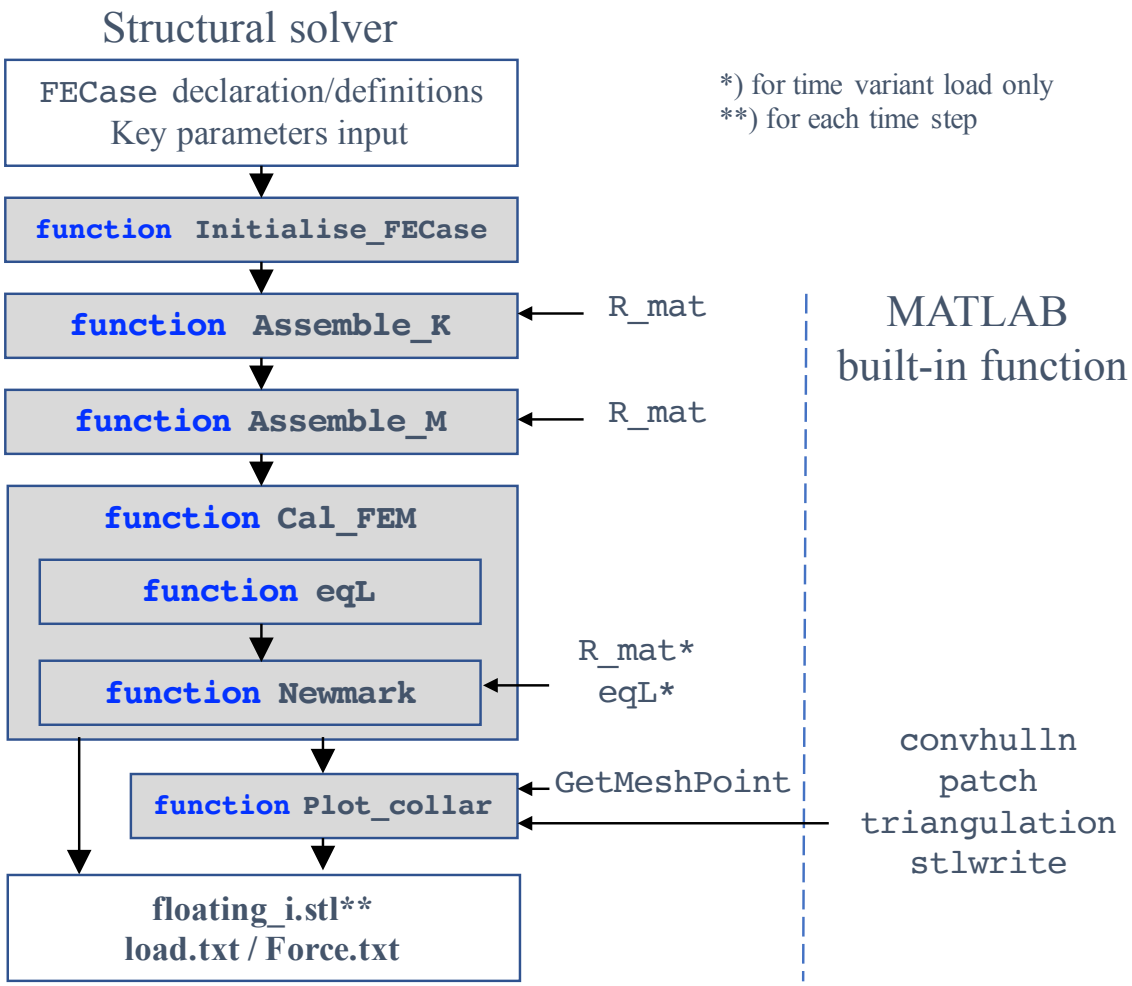


Figure 2.7: The structural solver work flow and functions

most negative (unstable) eigenvalue of a mass-spring system.

### 2.1.6 Structural solver work flow

The structural solver comprises several functions newly written and built-in functions from MATLAB library. The all the codes used for these functions are found in Appendix A. The following explains briefly what happen in each step of the work flow as illustrated in Figure 2.7.

- **Key parameters input**
  By using class definition in MATLAB, each calculation case will be handled as an individual class object. The class type object is called "FECase" here. Before setting-up one case, there are important input parameters to be defined such as

a cross section diameter, a collar diameter, the dimension of beam model, e.g. 2-D or 3-D beam, and the simulation end time.

- `Initialise_FECase function`
  This function basically sets up required parameter to perform the specific calculation. A number of variables are initially defined and set to zero if required. Both element-wise **K** and **M** matrices are defined here.

- `Assemble_K function`
  Each local stiffness matrix is assembled in this function. In order to perform this operation, a transformation of coordinate system is required in advance since every element will have its own orientation angle, considering circular type of collar structure.

- `Assemble_M function`
  Element-wise mass matrices should also be assembled in the same manner as the stiffness matrices. In case of static analysis, these matrices are ignored.

- `Cal_FEM function`
  This function comprises calculation parts of beam transient analysis. First of all, equivalent load should be identified and then the numerical scheme applies to the parameters to be calculated.

- `eqL function`
  The function introduces equivalent nodal loads from the results of shape function in case either a point load on midspan or a distributed along the beam. To be noted here is that this calculation case only assume vertical loads. Thus, this function should be updated if horizontal and lateral loads are concurrently considered.

- `Newmark function`
  This function includes a core part of this structural solver. Variables of functions can be a local type of variables for more flexibility in verifications and validations. If one has functional loads to be applied, which means time-variant loads, the loads should be defined within this function. However, constant load can be defined in the main body **m**-file, the outside of this function.

In order to check the input values, load data can be printed out this stage with respect to each node and time step. Forces and stresses are also tabulated for every nodes and time step.

- `Plot_collar function`
  This function performs several features. Firstly, the snapshots of collar structures can be found here and can be saved in the GIF format. Secondly, triangular meshes are identified and visualised. Lastly, triangular mesh data can be exported in a STL format.

- `R_mat function`
  As Figure 2.7 illustrated, this function is used in other functions like `Assemble_M` or `Assemble_K` and `Newmark`. This rotation can be explained by multilinear rotation where an origin of rotation has been preserved. Here, $n \times n$ matrix is introduced which is called "Rotation matrix". This matrix is orthogonal so the determinant of the matrix becomes 1.

- `GetMeshPoint function`
  A beam element inherently does not have volume but have axis vectors, which are solely 3-dimensional here, and cross section information. In this sense, some says the beam object in finite element method is regarded as 1-dimensional since meshing always takes place perpendicular to the axis vectors. In a 3-dimensional coordinate system, therefore, additional particular meshing is required to transfer the geometrical data to the fluid solver. In order to do that, this function defines position vector of the axis of each element. Then, two perpendicular vectors should be found to this (axis) position vector. By means of Rodrigues rotation, one could identify transformed point vectors with reference to the axis vector. By default, this function provides 16 mesh point per node, which is hard-coded.

- **Output files**
  To be noted is that STL format files are produced with a certain time interval. Apparently they can be printed out for each time step. Whereas, a load data file and forces/stresses data file contains the values for all the time steps.

## 2.2 Fluid Model

In this study, the open source CFD solver REEF3D is used to solve the governing equation of a fluid model. This section deals with the basic concepts of the computational methods employed in REEF3D.

REEF3D is an open-source CFD program developed at the Department of Civil and Transport Engineering with special focus on solving problems in the field of marine, coastal and ocean engineering, for example, the applications such as numerical wave tank, wave forces, breaking waves, floating body and open channel flow. It has been validated for a wide range of marine applications which are relevant for this thesis. [2] [14] From these studies the code showed a good agreement with experiments for the fluid and structure.

In particular, fluid flow problems with structures accompany non-linear effects due to wave steepness, non-linear wave-wave and wave-structure interactions. [13]
REEF3D employs the fifth-order WENO scheme for convection discretization and the level set method for obtaining a realistic representation of the free surface. These such a advanced numerical techniques - higher order discretization and the sharp representation of the free surface - enable users to achieve a more accurate modelling of waves.

The model describes the flow using incompressible RANS equations [4]. Turbulence is modelled with the two-equation $k-\omega$ model.

### 2.2.1 Reynolds-Averaged Navier Stokes Equations (RANS)

#### 2.2.1.1 Governing equations

To describe Computational Fluid Dynamics (CFD) simply, solving the RANS equations matters. The equations are derived from the continuity equation and the conservation of momentum equation under the assumption of an incompressible fluid.

The RANS equations provides a description of fluid flow:

$$\frac{\partial v_i}{\partial t} + v_j \frac{\partial v_i}{\partial x_j} = -\frac{1}{\rho}\frac{\partial p}{\partial x_i} + \frac{\partial}{\partial x_j}\left[\nu\left(\frac{\partial v_i}{\partial x_j} + \frac{\partial v_j}{\partial x_i}\right)\right] + g_i \tag{2.15}$$

where, $v$ is the velocity averaged over time $t$,
$\rho$ is the fluid density, $p$ is the pressure,
$\nu$ is the kinematic viscosity and $g$ is the gravitational acceleration.
$i, j$ are one coordinate direction and one another of a quantity varying.

where, $i$ is the direction to which the gravitational force applies, in particular.

#### 2.2.1.2 Solution to Navier-Stokes Equations : Projection Method

In order to solve Equation 2.15 one of important things to consider is to treat a non-linear term in the equation. Since Navier-Stokes equations are derived from the continuity equation and momentum conservation equation, it is inevitable to obtain a non-linear term in the equations.

The left hand side of Equation 2.15 has a set of convection terms while it has a diffusive term and source terms in the right hand side. However, there is no definition for the evolution of the pressure with respect to space. Thus, it is not possible to obtain even a numerical solution directly because one can not determine the pressure at the next grid point. Alternatively, the numerical model REEF3D offers some techniques for the treatment of the pressure term such as Projection Method.

$$\frac{\partial(v^* - v_i^n)}{\partial t} + v_j^n \frac{\partial v_i^n}{\partial x_j} = \frac{\partial}{\partial x_j}\left[\nu(\phi^n)\left(\frac{\partial v_i}{\partial x_j} + \frac{\partial v_j}{\partial x_i}\right)\right] + g_i \tag{2.16}$$

In the method proposed by Chorin [5], an intermediate velocity field is first obtained by ignoring the pressure gradient. A starting point is to consider the time-discrete RANS equations using a forward Euler scheme without pressure terms. Thus, it will explicitly obtain the solution $v_{n+1}$ at time $t_{n+1}$ from the solution of the previous time step $v_n$. One of the advantages of using this method is that the first step decouples the velocity and pressure field and computes an intermediate velocity field $v_i^*$ by omitting pressure gradient terms.

In the second step, the pressure can determine the velocity at time step $n+1$ since the equation has been decoupled as described in the previous step.

$$\frac{\partial(v_i^{n+1} - v_i^*)}{\partial t} + \frac{1}{\rho(\phi^n)} \frac{\partial p^{n+1}}{\partial x_i} = 0 \tag{2.17}$$

To solve Equation 2.17, one needs to know the pressure term because the term is still unknown. Here is called Poisson pressure equation by which one can calculate the pressure term. The formula is in the following:

$$\frac{\partial}{\partial x_i}\left(\frac{1}{\rho(\phi^n)} \frac{\partial p}{\partial x_i}\right) = \frac{1}{\Delta t} \frac{\partial v_i^*}{\partial x_i} \tag{2.18}$$

Then, the pressure value obtained from Equation 2.18 can be used in Equation 2.17 and eventually the velocity at the new time step can be obtained.

### 2.2.2 Spatial discretization

As mentioned in Section 2.2.1.2 the RANS equations comprise convective, diffusive and source terms. These terms need to be discretized first in order to solve the equations numerically. There are few schemes using finite difference in space such as First Order Upwind, Central Difference Scheme, Sharp and Monotonic Algorithm for Realistic Transport (SMART) and Weighted Essentially Non-Oscillatory (WENO) Scheme. The following paragraph will explain WENO scheme, employed by REEF3D. WENO is a non-oscillatory scheme therefore, it can be applied especially for a calculation where a higher stability is required with minimum risk. This method allows robust solutions and permits higher-order solutions at a point where a dramatic changes occurs in terms of physical quantities variation. This method fulfills the requirement of no overshoots or oscillations as well.

The first ENO scheme is given by Harten [8]. The third and fifth-order finite difference WENO schemes in a multi space dimension were constructed by Jiang and Peng [12], with a general framework for the design of the smoothness indicators and the nonlinear weights. An example of the implementation of this scheme in the Hamilton-Jacobi form to the level set function, $\phi_x$ in $x$-direction is presented as:

$$\phi_x = \begin{cases} \phi_x^- & \text{if } v_l > 0 \\ \phi_x^- & \text{if } v_l < 0 \\ 0 & \text{if } v_l = 0 \end{cases} \tag{2.19}$$

Where, $v_l$ is the velocity at a location. The WENO approximation for a given level set function is a combination of three possible approximations:

$$\phi_x^{\pm} = \omega_1 \phi_x^{1\pm} + \omega_2 \phi_x^{2\pm} + \omega_3 \phi_x^{3\pm} \tag{2.20}$$

The three ENO stencils defined for $\phi$ are formulated below:

$$\begin{aligned} \phi_x^{1\pm} &= \frac{q_1^{\pm}}{3} - \frac{7q_2^{\pm}}{6} + \frac{11q_3^{\pm}}{6}; \\ \phi_x^{2\pm} &= -\frac{q_2^{\pm}}{6} + \frac{5q_3^{\pm}}{6} + \frac{q_4^{\pm}}{3}; \\ \phi_x^{3\pm} &= \frac{q_3^{\pm}}{3} + \frac{5q_4^{\pm}}{6} - \frac{q_5^{\pm}}{6}; \end{aligned} \tag{2.21}$$

with,

$$q_1^- = \frac{\phi_{i-2} - \phi_{i-3}}{\Delta x}, q_2^- = \frac{\phi_{i-1} - \phi_{i-2}}{\Delta x}, q_3^- = \frac{\phi_i - \phi_{i-1}}{\Delta x}, \\ q_4^- = \frac{\phi_{i+1} - \phi_i}{\Delta x}, q_5^- = \frac{\phi_{i+2} - \phi_{i+1}}{\Delta x} \tag{2.22}$$

and,

$$q_1^+ = \frac{\phi_{i+3} - \phi_{i+2}}{\Delta x}, q_2^+ = \frac{\phi_{i+2} - \phi_{i+1}}{\Delta x}, q_3^+ = \frac{\phi_{i+1} - \phi_i}{\Delta x}, \\ q_4^+ = \frac{\phi_i - \phi_{i-1}}{\Delta x}, q_5^+ = \frac{\phi_{i-1} - \phi_{i-2}}{\Delta x} \tag{2.23}$$

the weights are written as:

$$\omega_1^{\pm} = \frac{\alpha_1^{\pm}}{\alpha_1^{\pm} + \alpha_2^{\pm} + \alpha_3^{\pm}}, \quad \omega_2^{\pm} = \frac{\alpha_2^{\pm}}{\alpha_1^{\pm} + \alpha_2^{\pm} + \alpha_3^{\pm}}, \quad \omega_3^{\pm} = \frac{\alpha_3^{\pm}}{\alpha_1^{\pm} + \alpha_2^{\pm} + \alpha_3^{\pm}}, \tag{2.24}$$

and

$$\alpha_1^{\pm} = \frac{1}{10}\frac{1}{(\tilde{\epsilon} + IS_1^{\pm})^2}, \quad \alpha_2^{\pm} = \frac{6}{10}\frac{1}{(\tilde{\epsilon} + IS_2^{\pm})^2}, \quad \alpha_3^{\pm} = \frac{3}{10}\frac{1}{(\tilde{\epsilon} + IS_3^{\pm})^2}, \tag{2.25}$$

where, the regularization parameter, $\tilde{\epsilon} = 10^{-6}$ and the following smoothness indicators:

$$IS_1^{\pm} = \frac{13}{12}(q_1 - 2q_2 + q_3)^2 + \frac{1}{4}(q_1 - 4q_2 + 3q_3)^2, \\ IS_2^{\pm} = \frac{13}{12}(q_2 - 2q_3 + q_4)^2 + \frac{1}{4}(q_2 - q_4)^2, \\ IS_3^{\pm} = \frac{13}{12}(q_3 - 2q_4 + q_5)^2 + \frac{1}{4}(3q_3 - 4q_4 + q_5)^2, \tag{2.26}$$

### 2.2.3 Time discretization

REEF3D provides with the 2nd order Adam-Bashforth, the third order- Total Variance Diminishing (TVD) and the fourth order Runge-Kutta schemes as time integration methods for the purpose of a higher accuracy, as fluid properties change swiftly with respect to the time. This study uses the third-order TVD Runge-Kutta scheme.

Third Order TVD Runge Kutta Scheme is an explicit 3rd order scheme which suppresses the oscillations of a numerical solution by controlling the local extrema [9].

An example of a such implementation is[20]:

$$\begin{aligned}\phi^{(1)} &= \phi^n + \Delta t L(\phi^n) \\ \phi^{(2)} &= \frac{3}{4}\phi^n + \frac{1}{4}\phi^{(1)} + \frac{1}{4}\Delta t L(\phi^{(1)}) \\ \phi^{n+1} &= \frac{1}{3}\phi^n + \frac{2}{3}\phi^{(2)} + \frac{2}{3}\Delta t L(\phi^{(2)})\end{aligned} \tag{2.27}$$

### 2.2.4 Turbulence modelling : $k-\omega$ Model

The $k-\omega$ model is a system of two-equation model based on the energy transport equations. One of the variables transported is the turbulent kinetic energy, $k$ and the other one is the turbulent dissipation, $\omega$. Then the eddy viscosity, $\nu_t$ is calculated by using $k$ and the $\omega$.(Equation 2.30) The transport equations for $k$ and $\omega$ are formulated as :

$$\frac{\partial k}{\partial t} + v_j\frac{\partial k}{\partial x_j} = \frac{\partial}{\partial x_j}[(\nu + \frac{\nu_t}{\sigma_k})\frac{\partial k}{\partial x_j}] + P_k - \beta_k k\omega \tag{2.28}$$

$$\frac{\partial \omega}{\partial t} + v_j\frac{\partial \omega}{\partial x_j} = \frac{\partial}{\partial x_j}[(\nu + \frac{\nu_t}{\sigma_k})\frac{\partial \omega}{\partial x_j}] + \frac{\omega}{k}\alpha P_k - \beta\omega^2 \tag{2.29}$$

$$\nu_t = c_\mu\frac{k}{\omega} \tag{2.30}$$

where, $P_k$ is the production rate and the closure coefficients $\sigma_k = 2, \sigma_\omega = 2, \alpha = \frac{5}{9}, \beta_k = \frac{9}{100}, \beta = \frac{3}{40}$.

### 2.2.5 Free surface modelling : Level Set Method (LSM)

A large collection of fluid problems involve moving interfaces such as air-water dynamics, breaking surface waves. In such applications, the interplay between the interface dynamics and the surrounding fluid motion is complex, with factors such as density ratios, temperature jumps across the interface, surface tension effects and boundary conditions playing significant roles in the dynamics. The free surface of water is modelled using a two-phase flow approach on a fixed Eulerian mesh. Aside from the interface, the level set function is a signed distance function:

$$\phi(\overrightarrow{x}, t)\begin{cases} > 0 & \text{if } \overrightarrow{x} \in \text{phase 1} \\ = 0 & \text{if } \overrightarrow{x} \in \Gamma \\ < 0 & \text{if } \overrightarrow{x} \in \text{phase 2} \end{cases} \tag{2.31}$$

Level set methods are computational techniques for tracking moving interfaces. They rely on an implicit representation of the interface whose equation of motion is numerically approximated using schemes built from those for hyperbolic conservation laws.

Thus, the level set function here in Equation 2.32 is coupled to the flow field with a pure convection equation:

$$\frac{\partial \phi}{\partial t} + v_j \frac{\partial \phi}{\partial x_j} = 0 \tag{2.32}$$

### 2.2.6 Wave generation

#### 2.2.6.1 Linear wave theory

In 1845, George B. Airy established a theory describing the wave kinematics and dynamics by using a first-order equation for surface gravity waves. According to this theory, which is also known as linear wave theory or small amplitude wave theory, continuity equation in Equation 2.34 will satisfy with Laplace equation if the velocity potential, $\Phi$, exists. Basically it has already been assumed that the fluid is homogeneous, inviscid, incompressible and irrotational to hold continuity equation. Horizontal and vertical velocities are denoted by $v$ and $w$, respectively. (A general case substitutes $x$ and $u$ for $y$ and $v$, respectively)

$$\frac{\partial \Phi}{\partial y} = v, \quad \frac{\partial \Phi}{\partial z} = w \tag{2.33}$$

$$\frac{\partial v}{\partial y} + \frac{\partial w}{\partial z} = \frac{\partial^2 \Phi}{\partial y^2} + \frac{\partial^2 \Phi}{\partial z^2} = 0 \tag{2.34}$$

To solve this Laplace equation, several assumptions and boundary conditions are introduced. [18] First of all, the bottom of the water column with a limited water dept is not permeable to the water, and therefore the vertical water velocity at the bottom must be zero at all times. At the closed bottom, accordingly:

$$w(y, z = -h, t) = \frac{\partial \Phi}{\partial z}(y, z = -h, t) = 0 \tag{2.35}$$

From the physical condition where a fluid particle at the surface should remain at the surface at all times, the following can be derived:

$$\frac{\partial \eta}{\partial t} + v \frac{\partial \eta}{\partial y} = w \tag{2.36}$$

Another physical condition in terms of dynamic behaviour of free surface is represented by Bernoulli's Equation. From this equation which deal with irrotational flow, the following can be derived at the surface $z = \eta$:

$$\frac{\partial \Phi}{\partial t} + \frac{1}{2}(v^2 + w^2) + g\eta = 0 \tag{2.37}$$

As mentioned above, there are additional assumptions to be considered to conclude the wave kinematics and dynamics in the following:

- Small amplitude, i.e. amplitude to wavelength ratio is supposed to be much smaller than 1
- Plane waves or long-crested (two-dimensional)

With these assumptions, those boundary conditions explained in Equation 2.35, 2.36 and 2.37 are linearized so that the variables can be summarised with respect to known parameters. Therefore, $\eta$, $\Phi$ and the dispersion relation in Equation 2.40 are obtained as follows:

$$\eta = asin(\omega t - ky) \tag{2.38}$$

$$\Phi = \frac{ag}{\omega}\frac{cosh(k(z+h))}{cosh(kh)}cos(\omega t - ky) \tag{2.39}$$

$$\omega^2 = gk \cdot tanh(kh) \tag{2.40}$$

#### 2.2.6.2 2nd order Stokes wave

2nd order Stokes wave is a way of representing non-linear waves. To tackle finite amplitude waves, this theory uses second order approximation. Stokes developed through the perturbation method to take into account the non-linear terms.
The second-order Stokes boundary value problem is governed by the Laplace equation in Equation 2.34 with both the kinematic and dynamic boundary conditions as well. In addition to these, the lateral boundary conditions and initial conditions are considered. Wave steepness is not used any longer in shallow waters to characterise the non-linearity of the waves. Therefore, the theory is applicable to deep waters and some range of intermediate waters. It formulates the wave characteristics in form of a power series of $\frac{H}{\lambda}$. The non-dimensional factor used in the power series are known as the perturbation factor. Here, $\eta$, $\Phi$, $v$ and $w$ can be described:

$$\eta = asin(\omega t - ky) + \frac{\pi H}{8}\frac{H}{\lambda}\frac{cosh(kh)(2+cosh2kh)}{sinh^3(kh)}cos2(ky - \omega t) \tag{2.41}$$

$$\Phi = \frac{ag}{\omega}\frac{cosh(k(z+h))}{cosh(kh)}cos(\omega t - ky) + \frac{3\pi cH}{16}\frac{H}{\lambda}\frac{cosh2k(h+z)}{sinh^4(kh)}sin2(ky - \omega t) \tag{2.42}$$

where, $c = \frac{\omega}{k}$

$$v = \frac{\partial \Phi}{\partial y} = a\omega\frac{coshk(z+h)}{sinh(kh)}sin(ky+\omega t) + \frac{H}{\lambda}\frac{3\pi^2 H sinh2k(h+z)}{4Tsinh^4(kh)}cos2(ky-\omega t) \tag{2.43}$$

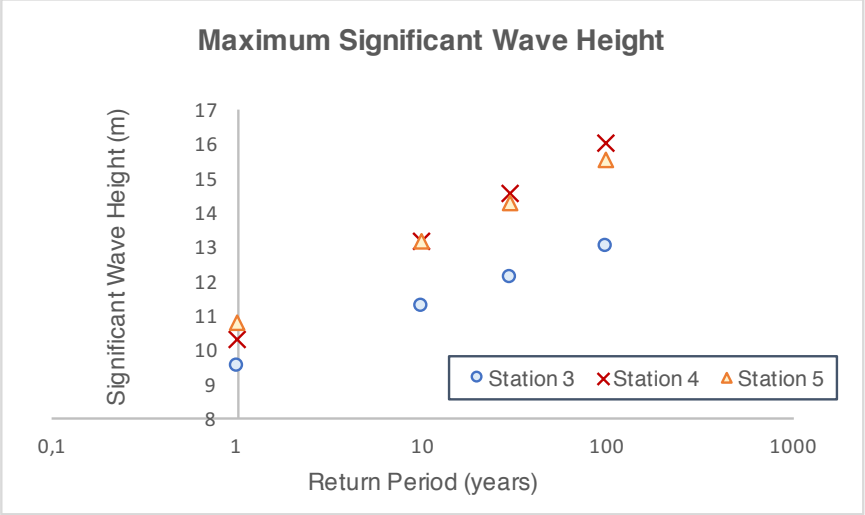


Figure 2.8: Maximum Significant Wave Height in the North Sea on the Norwegian Continental Shelf [22] (Sta. No. 3: 3.21E, 60.49N; 4:2.07E, 60.88N, 5:7.17E, 65.14N)

$$w = \frac{\partial \Phi}{\partial z} = a\omega \frac{coshk(z+h)}{sinh(kh)} sin(ky+\omega t) + \frac{H}{\lambda} \frac{3\pi^2 H cosh2k(h+z)}{4Tsinh^4(kh)} sin2(ky-\omega t) \quad (2.44)$$

In this thesis, 2nd order Stokes waves are generated and used in numerical wave tanks.

#### 2.2.6.3 Wave height

Generally a wave height to apply to the analyses is estimated based on preferably actual measurements since extreme wave loading could limit the design and determine the dimension of structures. From a literature review [22], where actual measurements were carried out for several stations in the Norwegian Continental Shelf, it is found that the Station 3 and 4 are close to Bergen and the Station 5 is located in front of Trondelag region, from both of which lots of aquaculture activities are ongoing.

Figure 2.8 is plotted based on regression data from the literature, e.g. maximum significant wave height for 1 year and 100 years of return period, and an estimation under the assumption that the maximum significant wave height follow Weibull distribution. e.g. the values for 10 and 50 years of return period.

Considering the regression trend line in the literature ended with year 1999 and the wave values increase as the reference year goes by, there is an uncertainty by which the reading as of 2019 can be overrated.

Another thing to consider is a return period. From a piece of information [3] about the material lifetime of 50 years in HDPE's case, the expected life time for aquaculture structure is less than that and the life cycle for net structure is much less than

that e.g. 4 to 6 years for nylon and 14 years for polyethylene terephthalate [3]. Thus, 30 years of return period is assumed to be a lifetime of a whole aquaculture structure. As a result, it is assumed that 10 m of maximum wave height is probable considering the life time of aquaculture structure and uncertainties in the prediction. Moreover, it is a fact that stations in the article are farther offshore compared to popular aquaculture sites. Thus, this value will be used as an extreme case loading and it would not be reasonable to employ a higher wave height than this. Also, 5 m and 0.6 m of wave heights will also be presented as a more credible loading case. Therefore, three wave height values will be used as input parameter of the presentation of the fluid model.

### 2.2.7 Numerical Wave Tank

In order to design or analyse an ocean and coastal engineering problem, a numerical wave tank (NWT) can be an useful tool as a part of a numerical model which can be an alternative to physical modelling. Numerical wave tanks can work with diverse ocean and coastal engineering structures or obstacles.
In this thesis, to elaborate the collar model set-up in a numerical wave tank, a 2-dimensional horizontal cylinder is modelled and presented in advance. The detail information about these preparations is found in Section 3.2.

# Chapter 3

# Results

This thesis yields the results which comprise a set of validations for the structural solver and a series of presentations for the fluid model with rigid body structures. This chapter does not provide with any validation only for the fluid solver, because a number of validations have already been carried out with this CFD code to verify free surface flow and its effect on structure. [13] [19]

## 3.1 Validation of Structure Solver

For transient analysis, the dynamic equation in Equation 2.1 is numerically solved by the Newmark scheme as mentioned above. The results between the structural solver and a commercial tool have been compared in case the exact solution is not easily derived.
From a chronological order of development of this solver, it is more logical and natural that the static analysis should be checked prior to a validation the dynamic analysis in order to make sure of element connectivity and stiffness matrix.
The following section explains 2-dimensional("2-D") beam model analysed by static equation first and a comparison with examples from Bathe [1]. Lastly, dynamic analyses for a 3-dimensional beam model have been validated with the results from ANSYS Mechanical APDL 19.1, hereafter also referred as "ANSYS".

### 3.1.1 2 - dimensional beam model static analysis

This section explains about a static analysis. A simple formula below can summarise what the analysis incorporates:

$$\left[\mathbf{K}\right]\mathbf{u} = \mathbf{F} \tag{3.1}$$

Table 3.1: Input parameter for 2-D Beam validation with exact solutions

| Properties | | Unit | Value |
|---|---|---|---|
| The number of element | $n$ | - | up to more than 30 |
| Beam Object | - | - | 2D |
| Element length | $L$ | $m$ | 1.0 |
| Point load | $P$ | $N$ | 1000 |
| Distributed load | $q$ | $N/m$ | 100 |
| Sectional Area | $A$ | $m^2$ | 1 |
| Bending Stiffness | $EI$ | $Nm^2$ | $1e+3$ |

where, **u** is a displacement vector along the corresponding domain.

**K** is a stiffness matrix and **F** is a force (or load) vector.
In order to find the displacement vector, the inverse matrix of **K** should be multiplied to the left side of the force vector. However, the **K** is singular so this matrix is not invertible. By means of Gauss Elimination - also known as row reduction or row striking-, therefore, a part of the stiffness matrix becomes invertible so that the displacement can be evaluated.
Input values used in this validation case are summarised in Table 3.1, where the values are not realistic values.

#### 3.1.1.1 Distributed load

In case a distributed load applies along with a beam, bound by one end, i.e. cantilever, the exact solution of vertical displacements, $\mathbf{w}(x)$, can be derived in the following as a function of $x$, horizontal distances:

$$\mathbf{w}(x) = \frac{q}{24EI}x^2(x^2 + 2L(3L - 2x)) \tag{3.2}$$

$EI$: Bending stiffness in $Nm^2$,
$q$ : Distributed load in $N/m$,
$L$ : Length of the beam in $m$

In Figure 3.1a and 3.1b, exact solutions were compared to the numerical solutions by the solution of the structure solver. The orders of error in these cases were $10^{-14}$ and $10^{-13}$ when the number of element, $n$, is 2 and 4, respectively.
In this load case, the amount of errors can be negligible. It implies that possibly the error occurred due to computation limitation e.g. an error induced by round-off. To conclude, the almost same value has been obtained by two different calculations by

the exact hand calculation and by the structural solver, for the distributed load cases.

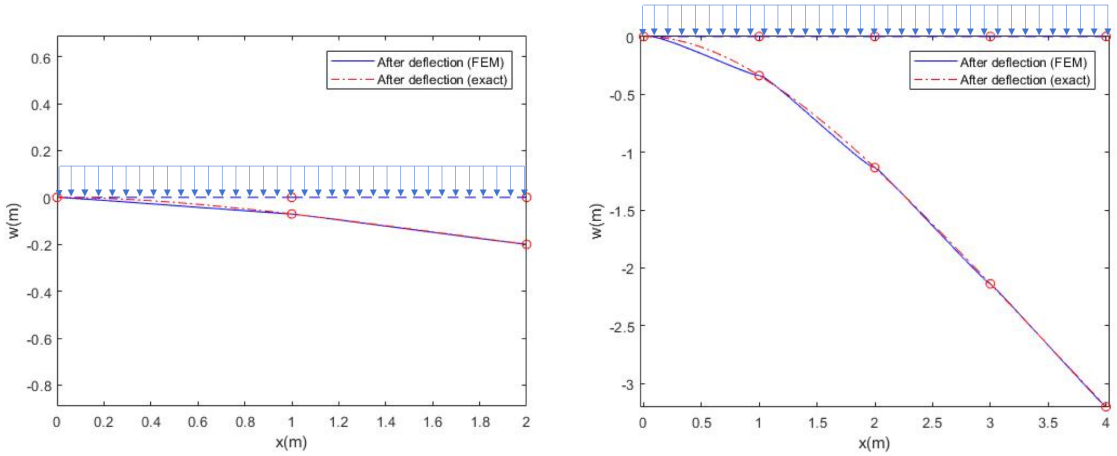


(a) Distributed load (n=2) (b) Distributed load (n=4)

Figure 3.1: Distributed load on cantilever (Exact solution vs. Structural solver)

#### 3.1.1.2 Point load at midspan

When a point load applies to the midspan of the cantilever beam, the exact solution of the vertical deflection can be obtained by:

$$\mathbf{w}(x) = \frac{FL^2}{24EI}(3x - \frac{L}{2}) \qquad ,when \quad x > \frac{L}{2} \tag{3.3a}$$

$$\mathbf{w}(x) = \frac{Fx^2}{6EI}(\frac{3L}{2} - x) \qquad ,when \quad x < \frac{L}{2} \tag{3.3b}$$

The order of errors in these cases might not be disregarded since they are maximum 2.2 % and 0.2 % when the number of element, $n$, is 3 and 9, respectively. This is under the expectation because only errors occurred in the free end side - a half of right hand side - from the location where the point load is applied. Thus, this is certainly caused by the un-defined angle of the free end.
In case the number of element are even getting greater than 9, one can find the order of error becoming smaller. Figure 3.3 shows that the magnitude of error becomes exponentially smaller as the number of elements become larger.

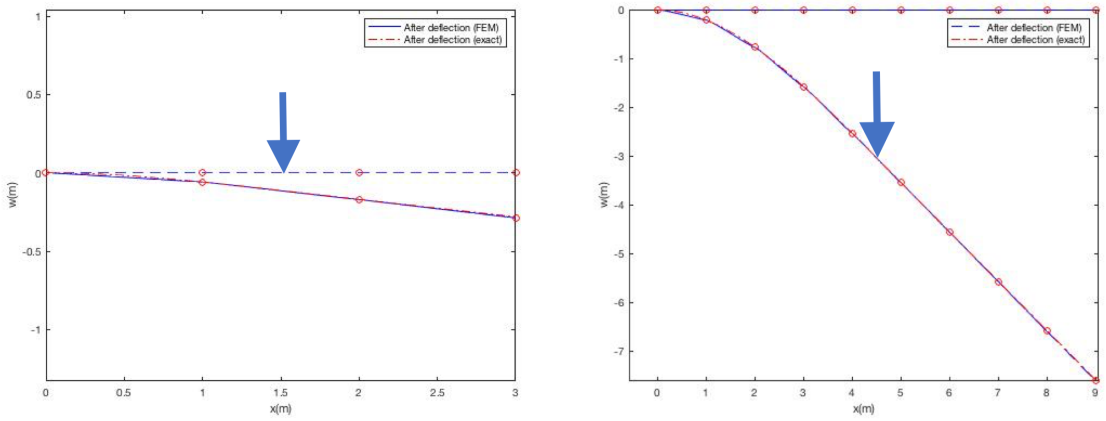


(a) Point load (n=3) (b) Point load (n=9)

Figure 3.2: Point load at midspan of cantilever (Exact solution vs. Structural solver)

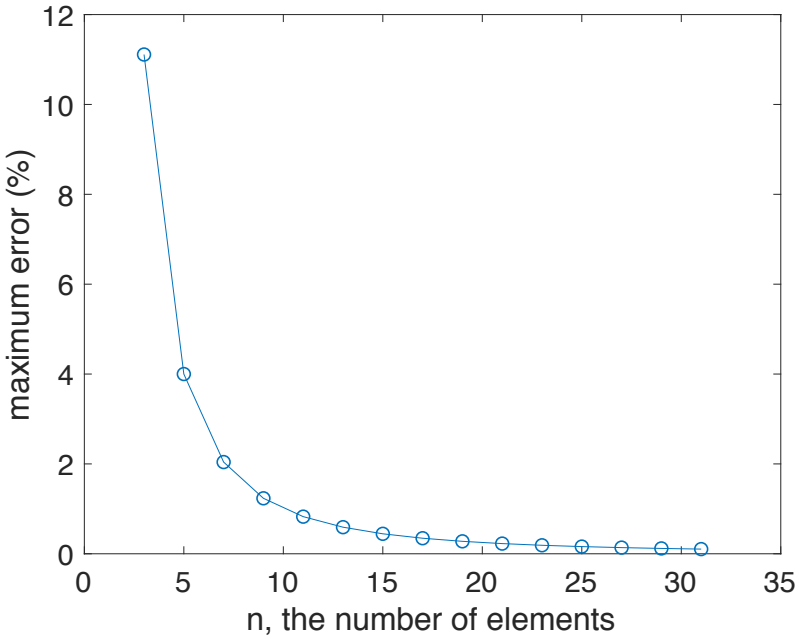


Figure 3.3: Convergence check for errors in point load at midspan case

### 3.1.2 Differential equations from Bathe

There are limited number of sources that one can refer to while validating the results of the newly developed solver here in the study. Bathe [1] demonstrated the numerical solution of few differential equations by Newmark scheme, which is thought as reliable.

#### 3.1.2.1 Decoupled two differential equations

The example case equation is described as below:

$$\begin{aligned} \ddot{u}_1 + 2u_1 &= \frac{10}{\sqrt{3}} \\ \ddot{u}_2 + 5u_2 &= -10\sqrt{\frac{2}{3}} \end{aligned} \tag{3.4}$$

This validation case is focusing on the numerical scheme itself rather than the finite element method. Thus, the Newmark scheme were computed by this thesis work and this plot is compared with the solution from Bathe, where "Newmark by Sung" in the legend of Figure 3.4 means the one developed for this thesis and "Newmark by Bathe" in the legend of the same figure stands for Bathe's solutions.
Figure 3.4 shows a good agreement among the computed schemes and Bathe's solution.

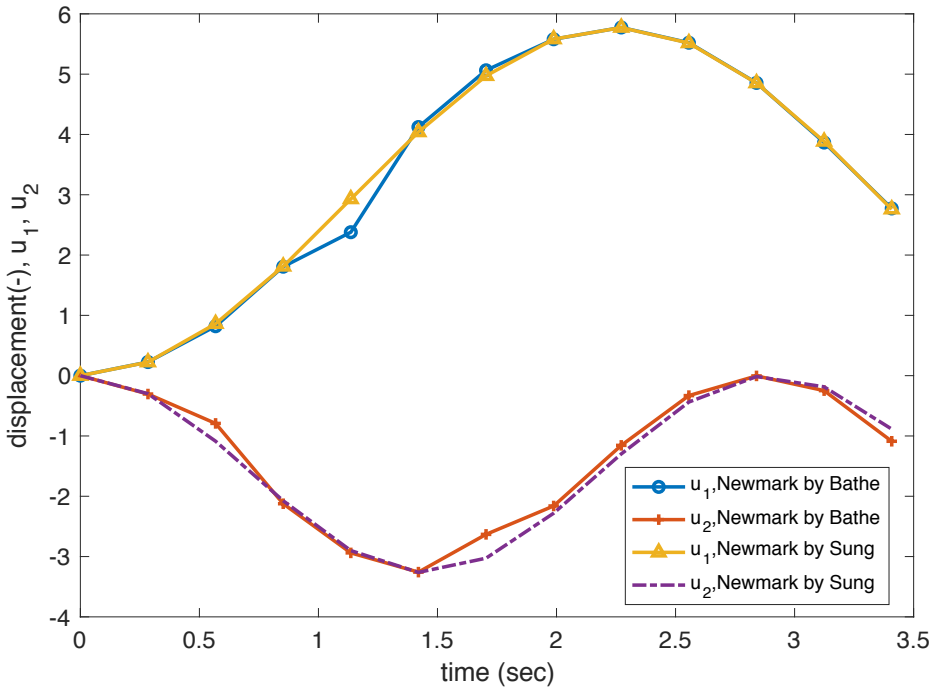


Figure 3.4: Decoupled two differential equations

#### 3.1.2.2 Coupled differential equations

Equation 3.5 described the coupled differential equations.

$$
\begin{aligned}
2\ddot{u}_1 + 6u_1 - 2u_2 &= 0 \\
\ddot{u}_2 - 2u_1 + 4u_2 &= 10
\end{aligned} \tag{3.5}
$$

Figure 3.5 also shows that the computed numerical schemes have a good agreement with Bathe's computation by Newmark scheme.

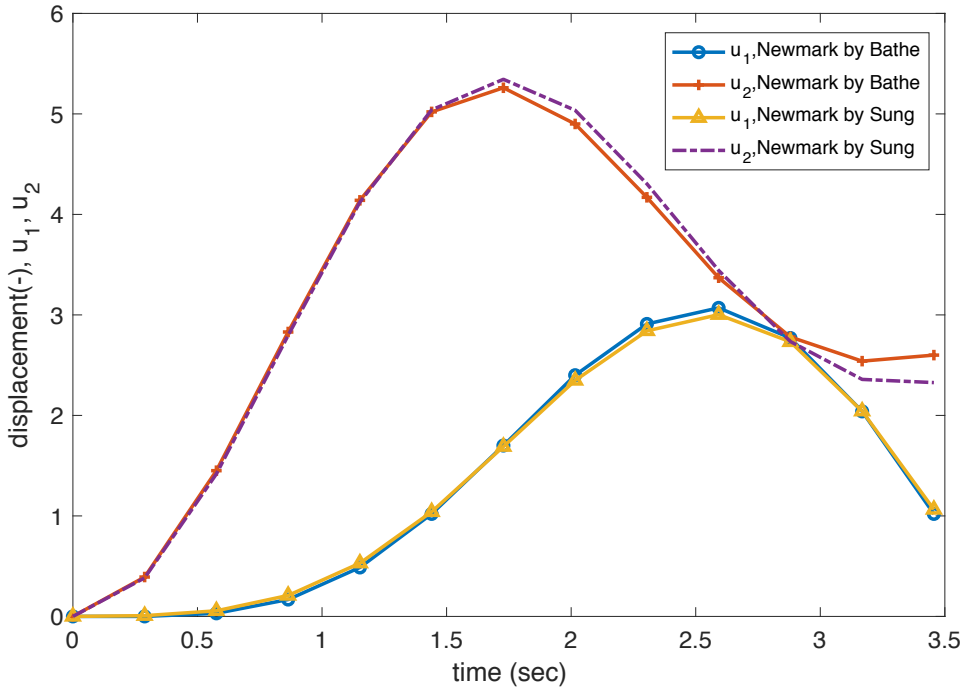


Figure 3.5: Coupled differential equations

### 3.1.3 Structural dynamic analysis

From the precedent sections a set of validations has proved the structural solver's accuracy and the capability to deal with ordinary differential equation as described in Section 3.1.2. With respect to the performance for the structural dynamic analysis aiming at structural dynamics of the collar, a 3-dimensional beam model is eventually required to be validated. That is because the 3-dimensional model will be coupled to the fluid solver and the data will be transferred in both ways between the fluid solver and the structural solver for investigating fluid-structure interaction in future work. Now, the validation work is concentrating on a 2-dimensional and 3-dimensional can-

tilever case, 5 meter long and forced by either a point load at a free end or distributed load along the beam.

Due to the fact that it is difficult to find a proper exact solution of 3-dimensional beam dynamic analysis, a series of transient analysis were compared with the result from a commercial code, ANSYS, varying a number of combination of input parameters such as time step and the number of elements.
This validation case is so "stiff", which means relatively high bending stiffness in a physical context, $EI \approx 1e+8$ or $1e+9$. At the same time, it implies a high ratio between the largest eigenvalue and the smallest one in a mathematical context that is why a high frequent vibration is captured even though one pushes down the free end of the cantilever beam steadily. In addition, a very small time step, e.g. $1e-05$ or $1e-06$, is required to obtain a reliable solution which fits the corresponding result from ANSYS. As a result, these validations from the structural solver, denoted by "MATLAB Newmark" in the legend, yields a good agreement in terms of amplitudes and its phase within order of negligible level if one can choose a proper time step associated with the number of element.

#### 3.1.3.1 Input parameter

Table 3.2 summarises the input parameters that have been used in the validations.
*) BEAM3 and BEAM4 are objects from ANSYS

Table 3.2: Input parameter for validations with ANSYS

| Properties | | Unit | Value |
|---|---|---|---|
| Time steps | $\Delta t$ | $s$ | 1e-04, 1e-05, 1e-06 |
| The number of element | $n$ | - | 5, 20, 60, 80 |
| Beam Object | - | - | 2D(BEAM3*), 3D(BEAM4*) |
| Total length | $L$ | $m$ | 5.0 |
| Diameter | $D$ | $m$ | 0.2 |
| Density | $\rho$ | $kg/m^3$ | 7850 |
| Point load | $P$ | $kN$ | 0.1 or 1 |
| Distributed load | $q$ | $kN/m$ | 0.1 |
| Shear Modulus | $G$ | $Pa = N/m^2$ | $7.692e+10$ |
| Poisson's ratio | $PR$ | - | 0.3 |
| Sectional Area | $A$ | $m^2$ | 0.0314 |
| Young's Modulus | $E$ | $Pa = N/m^2$ | $2e+11$ |
| Area moment of inertia | $I$ | $m^4$ | $7.854e-3$ |

In the following sections, errors from either 2 or 3 dimensional beam model valida-

tions are tabulated where the both beams are either forced by a point load and a distributed load. The number of element, $n$, plays a role of one variable since it affects the accuracy.

The definition of error (or integration error) can be altered by the difference between two results from respective Newmark method e.g. by the structural solver for this thesis work and by ANSYS since no available exact solution exists. When the errors are presented, the ratios are calculated from the absolute errors over the corresponding ANSYS results as a reference to make them be non-dimensionalised. Table 3.3, 3.4, 3.5 and 3.6 were tabulated to present errors in percentage.

#### 3.1.3.2 Point load at 2-D Beam

In case of a point load applying at a free end of a 2-dimensional beam, a vibration is captured as explained in Section 3.1.3. 100 N of the point load is applied and Figure 3.6 presents the vertical displacement with respect to simulation time. The beam properties are stipulated in Table 3.2.

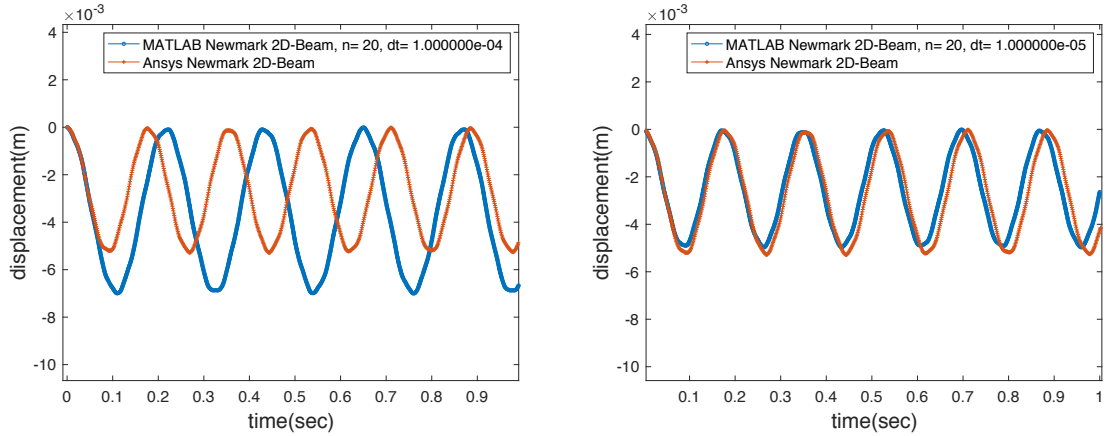


(a) $\Delta t = 1E-04s$ (b) $\Delta t = 1E-05s$

Figure 3.6: Transient solution of the 2-D Beam with a point load (n=20)

Compared to Figure 3.6b, however, Figure 3.6a does not show a good fit between two solutions by MATLAB and ANSYS in terms of the amplitudes and the phase errors. However, the solution looks not unstable even though it is less accurate. In case the number of element is 20, less than 1e-05 of time step would produce way accurate results than any other longer time step cases.

Overall, the convergence against time steps has been observed since the accuracy has improved as time steps are reduced. When the beam has a very limited number of elements e.g. 5, however, the improvement of the accuracy for transient solutions

is stagnated for even shorter time step than 1e-05 second as shown in 19% and 13% for amplitude error and phase error, respectively.

Table 3.3: Summary of errors, 2D-Beam, Point load

| Category | $n$ | Error | | | | |
|---|---|---|---|---|---|---|
| Time step<br>The number of time steps | | 1e-03<br>1e+3 | 1e-04<br>1e+04 | 1e-05<br>1e+05 | 1e-06<br>1e+06 | 1e-07<br>1e+07 |
| Amplitude error | 5 | 82% | 17% | 19% | 19% | 19% |
| | 20 | 100% | 39% | 4% | 4% | 4% |
| | 60 | 100% | 243% | 2% | 0% | |
| Phase error | 5 | 42% | 11% | 13% | 13% | 13% |
| | 20 | 462% | 21% | 1% | 2% | 1% |
| | 60 | 462% | 105% | 1% | 0% | |

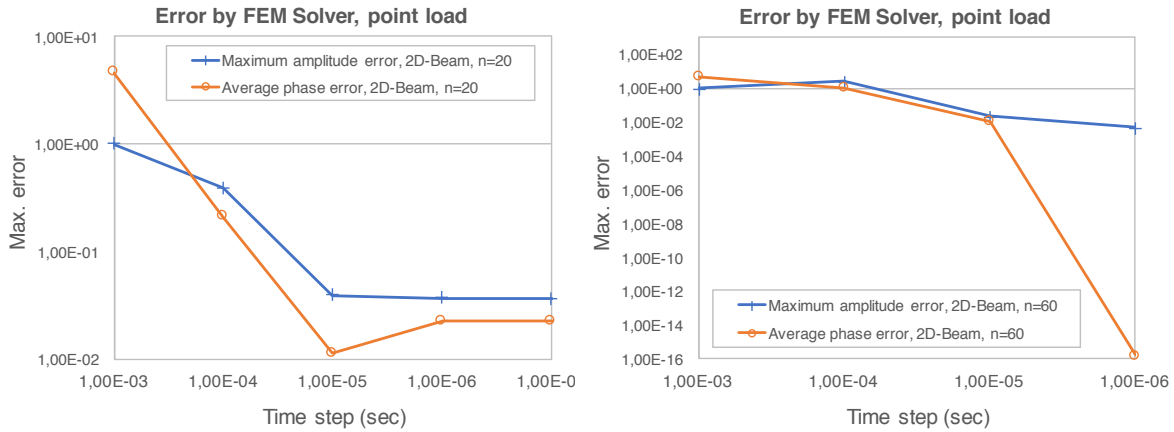


(a) Point load (n=20)

(b) Point load (n=60)

Figure 3.7: Errors by the structural solver compared to ANSYS, 2-D Beam, Point load

### 3.1.3.3 Distributed load along 2-D Beam

When a distributed load, 100 $N/m$, applies along the 2-dimensional beam, bound by one end, e.g. cantilever, the global patterns of transient solution is similar to that of point load case in Section 3.1.3.2. In general, the amounts of errors are slightly greater than those of point load cases as shown in Table 3.4.
Table 3.4 and Figure 3.10 present the errors induced by the structural solver compared to ANSYS results.

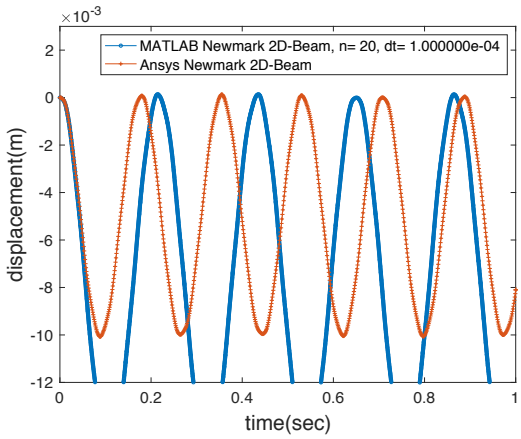


(a) $\Delta t = 1E-04s$

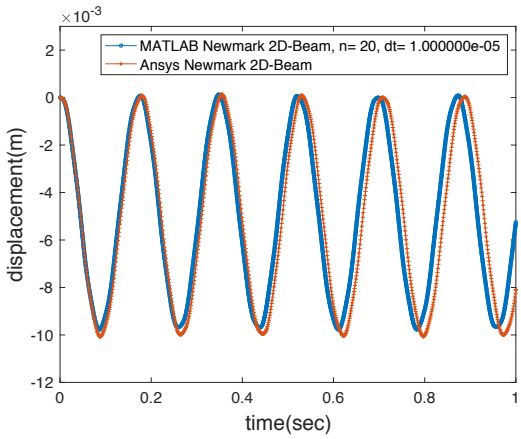


(b) $\Delta t = 1E-05s$

Figure 3.8: Transient solution of the 2-D Beam with distributed load (n=20)

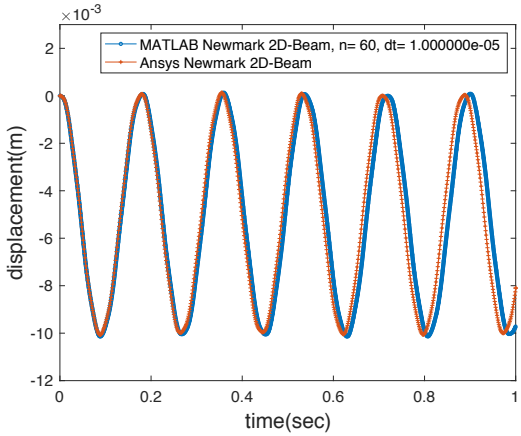


(a) $\Delta t = 1E-05s$

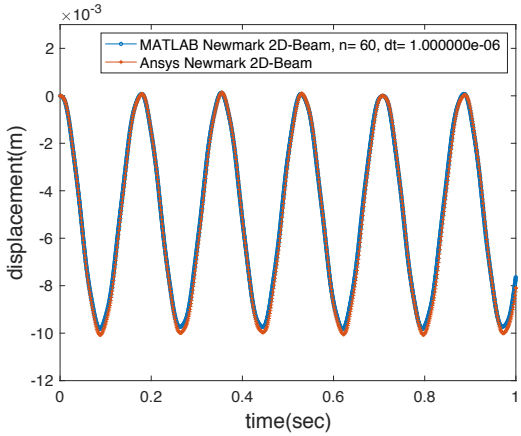


(b) $\Delta t = 1E-06s$

Figure 3.9: Transient solution of the 2-D Beam with distributed load (n=60)

Table 3.4: Summary of errors, 2D-Beam, Distributed load

| Category | $n$ | Error | | | | |
|---|---|---|---|---|---|---|
| Time step<br>The number of time steps | | 1e-03<br>1e+3 | 1e-04<br>1e+04 | 1e-05<br>1e+05 | 1e-06<br>1e+06 | 1e-07<br>1e+07 |
| Amplitude error | 5 | 102% | 20% | 21% | 21% | 21% |
| | 20 | 100% | 50% | 3% | 4% | 4% |
| | 60 | 100% | 322% | 4% | 0% | |
| Phase error | 5 | 44% | 11% | 13% | 13% | 13% |
| | 20 | 468% | 22% | 2% | 2% | 2% |
| | 60 | 468% | 107% | 2% | 0% | |

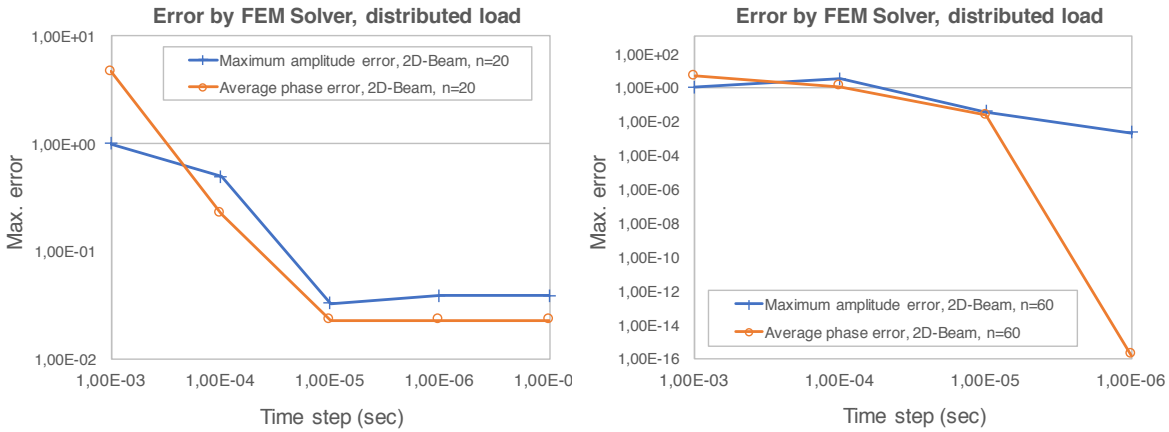


(a) Distributed load (n=20)

(b) Distributed load (n=60)

Figure 3.10: Errors by the structural solver compared to ANSYS, 2-D Beam, Distributed load

#### 3.1.3.4 Point load at 3-D beam

A 3-dimensional("3-D") beam has inherently different properties such as 6 of the number of degree of freedom per node while a 2-dimensional beam has 3 per node. Input parameters for 3-dimensional beams are identical to those for 2-dimensional cases as shown in Table 3.2.

Table 3.5: Summary of errors, 3-D Beam, Point load

| Category | $n$ | Error | | | | |
|---|---|---|---|---|---|---|
| Time step<br>The number of time steps | | 1e-03<br>1e+3 | 1e-04<br>1e+04 | 1e-05<br>1e+05 | 1e-06<br>1e+06 | 1e-07<br>1e+07 |
| Amplitude error | 20 | 1878% | 10% | 9% | 10% | - |
| | 60 | 1000% | 154% | 0% | 3% | - |
| | 80 | - | - | - | - | - |
| Phase error | 20 | 417% | 6% | 7% | 7% | - |
| | 60 | 417 | 74% | 0% | 1% | - |
| | 80 | - | - | - | - | - |

Table 3.5 summarises integration errors produced by 3-D Beam structural dynamic analyses compared with ANSYS analyses. One thing to be noted here is that the minimum level of error, about 10% in amplitude, from all the number of time step cases computed is greater than that of 2-D cases which is around 4%, comparing 20 of the number of elements.

Thus, 3-D analyses are more likely to require such a sufficiently larger number of elements in order for a certain case to be calculated. Surely, even with such that number of element, the time step should be sufficiently small to conduct the case.

One thing to be noted in Figure 3.12 is that the best fit can be produced by a

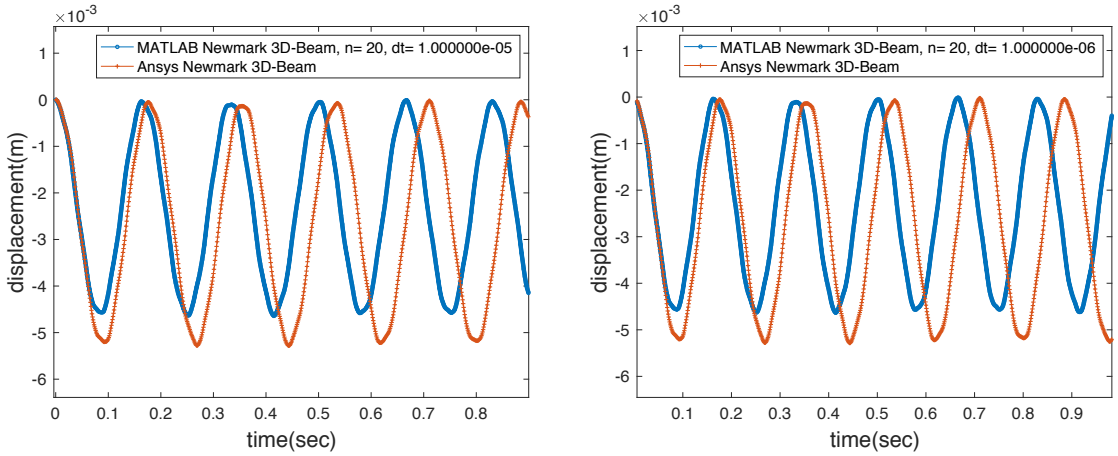


(a) $\Delta t = 1E-05s$ (b) $\Delta t = 1E-06s$

Figure 3.11: Transient solution of the 3-D beam with a point load (n=20)

computation with a more longer time step. One might think that it is strange when even a smaller time step yields less accurate solution. That is because, however, it might be more related to mode of vibrations. [1]

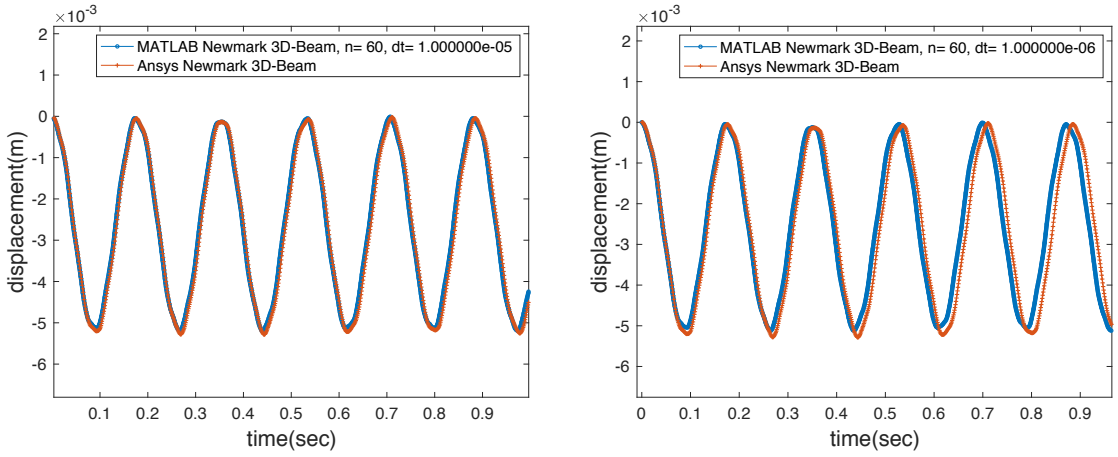


(a) $\Delta t = 1E-05s$ (b) $\Delta t = 1E-06s$

Figure 3.12: Transient solution of the 3-D beam with a point load (n=60)

#### 3.1.3.5 Distributed load along 3-D Beam

Lastly, a distributed load along the 3-D Beam has been applied to validate the results with the ANSYS results. Table 3.6 presents the summary of errors in this set of validations.

Table 3.6: Summary of errors, 3-D beam, Distributed load

| Category | $n$ | Error | | | | |
|---|---|---|---|---|---|---|
| Time step<br>The number of time steps | | 1e-03<br>1e+3 | 1e-04<br>1e+04 | 1e-05<br>1e+05 | 1e-06<br>1e+06 | 1e-07<br>1e+07 |
| Amplitude error | 20 | 2432% | 14% | 12% | 12% | 12% |
| | 60 | 100% | 204% | 1% | 3% | |
| | 80 | 100% | 304% | 2% | 2% | |
| Phase error | 20 | 423% | 7% | 6% | 6% | 6% |
| | 60 | 468 | 78% | 0% | 2% | |
| | 80 | 468% | 105% | 1% | 0% | |

One similar thing to point load cases is lower overall accuracy compared to that of 2-D cases when one can be notified by looking up the case where the number of elements is 20.

So far the validation with ANSYS results have been carried out. There is, however,

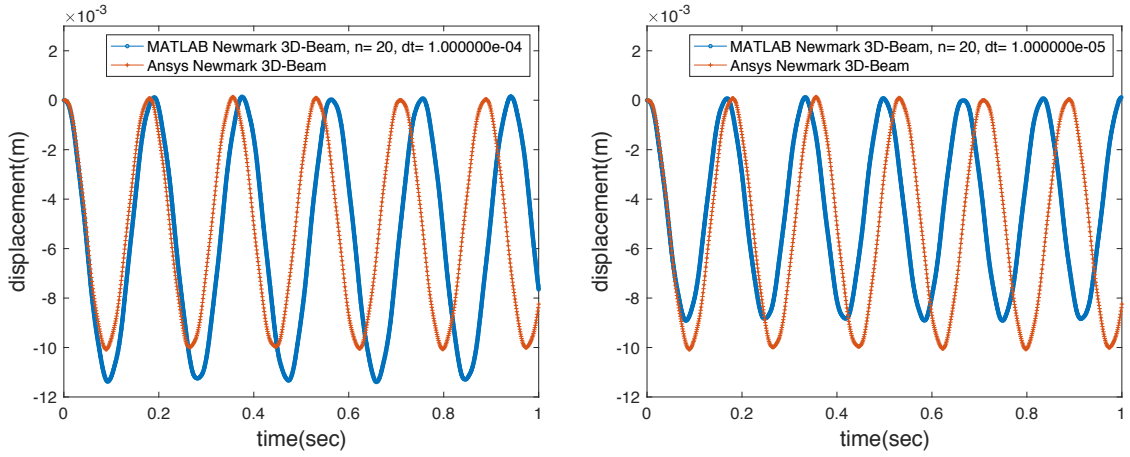


(a) $\Delta t = 1E-04s$ (b) $\Delta t = 1E-05s$

Figure 3.13: Transient solution of the 3-D Beam with distributed load (n=20)

an uncertainty about the accuracy with respect to parameters like the time steps and the number of elements. This uncertainty is induced by several features to make the results of ANSYS more accurate, which might be set by default values, regardless of

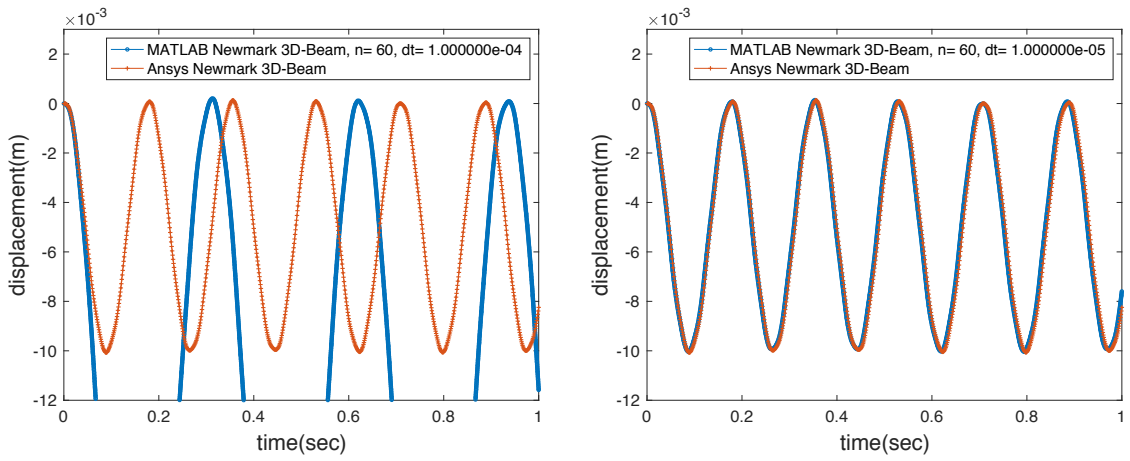


(a) $\Delta t = 1E-04s$ (b) $\Delta t = 1E-05s$

Figure 3.14: Transient solution of the 3-D Beam with distributed load (n=60)

these parameters. Nonetheless, to discover the reason in detail is not a purpose of this thesis thus it is assumed that the result of ANSYS is sufficiently accurate by the verification of those ANSYS results varying a number of elements.

### 3.1.4 Collar drop simulation

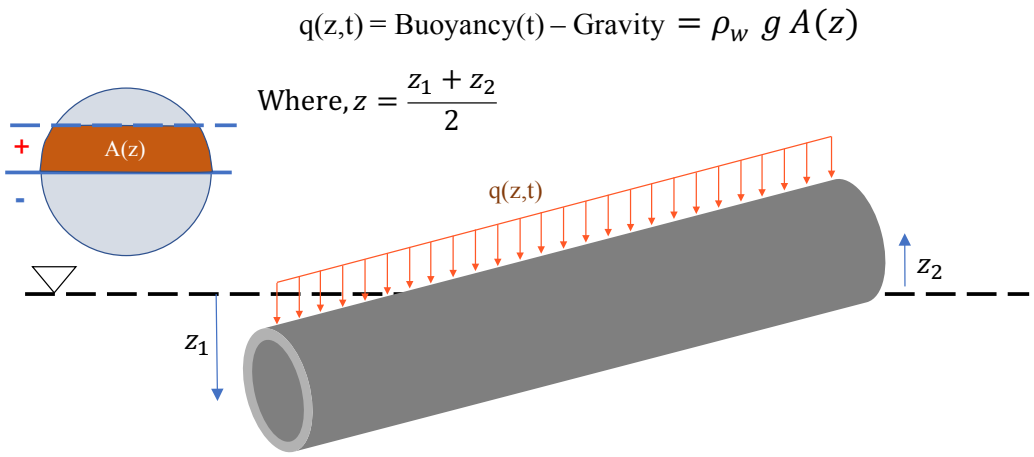


Figure 3.15: Buoyancy and gravity force

In this section, vertical displacements from respective nodes can be captured by the structural solver with respect to time. These series of simulations figure out how the

model and actual structures behaviours would be alike. $1e-03\ s$ of time step is used since HDPE material is less stiff than steel material. Here, buoyancy function is defined and applied with gravity force to the right hand side of Equation 2.1 as a time-variant force. Figure 3.15 and Equation 3.6 shows how the forces are calculated by measuring the average draft of every element.

$$A(z) = 2R^2(sin^{-1}(\frac{z}{R}) + \frac{1}{2}sin(2sin^{-1}(\frac{z}{R}))) \tag{3.6}$$

Where, $R$ : Outer radius of pipe, $z = \frac{z_1+z_2}{2}$.

#### 3.1.4.1 1m of initial displacement

In case all the nodes have the same initial displacement of 1 $m$, the collar bounces back by buoyancy force while keeping its original shape as if it is a rigid body. Thus, all the nodes have the same trajectory with respect to time.

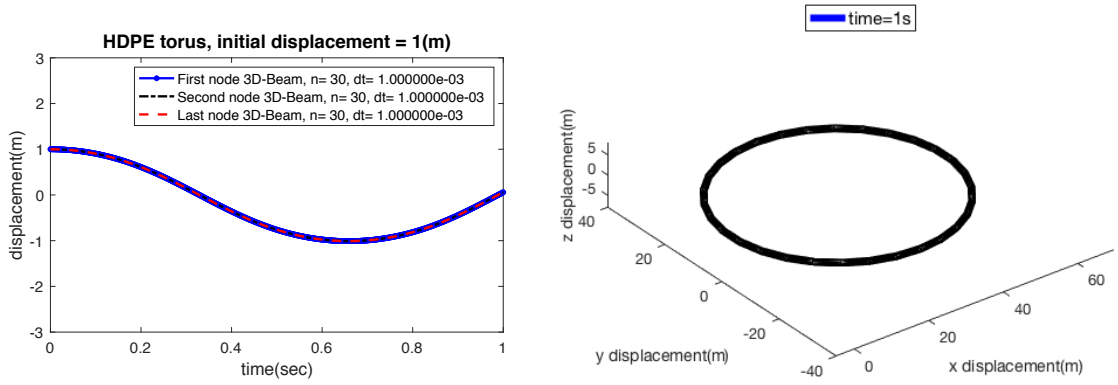


(a) Vertical trajectory for nodes

(b) Snapshot of collar (t=1s)

Figure 3.16: Collar drop for 1 m of initial displacement

#### 3.1.4.2 1 to 4 m of initial displacement

In this presentation case, every node has its own initial displacement, which gradually increases by the order of nodes.

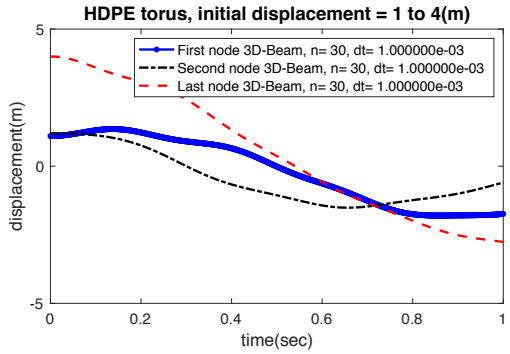


(a) Vertical trajectory for nodes

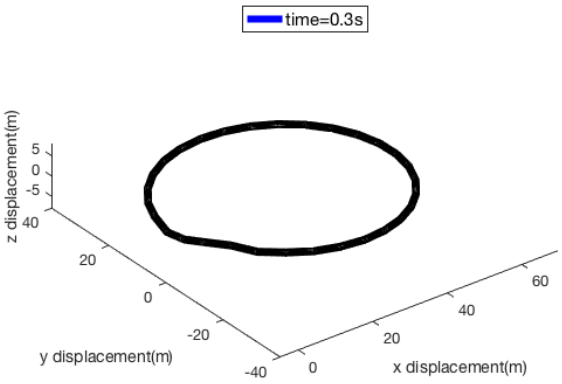


(b) Snapshot of collar (t=0.3s)

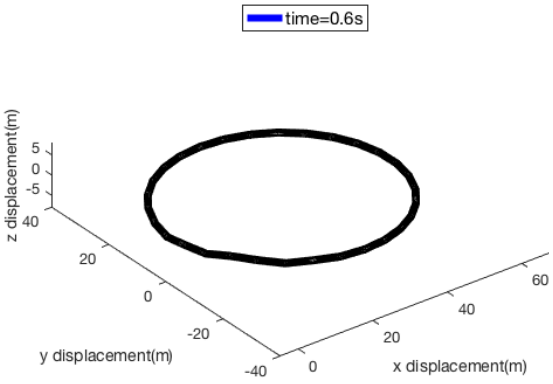


(c) Snapshot of collar (t=0.6s)

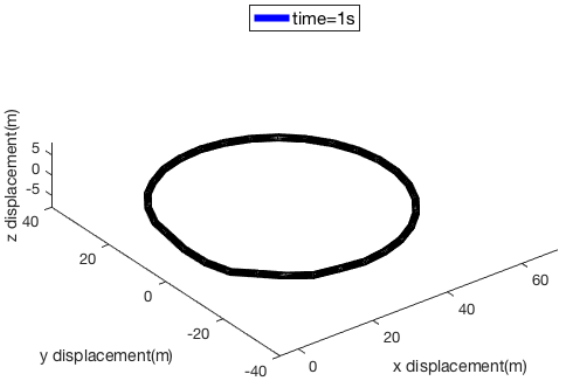


(d) Snapshot of collar (t=1.0s)

Figure 3.17: Collar drop from 1 to 4m of initial displacement

#### 3.1.4.3 -3 to 3 m of initial displacement

This case presents more extreme case, where the initial displacement of one to another is 6 $m$ of difference. In this assumption, more modes of vibrations are observed as shown in Figure 3.18a.

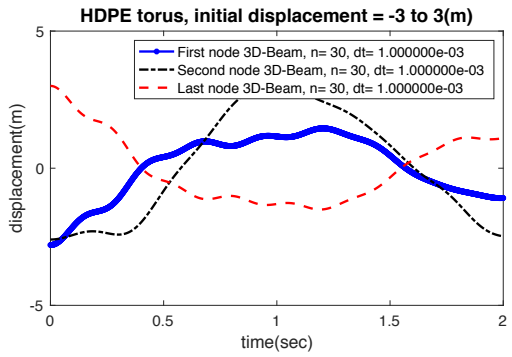


(a) Vertical trajectory for nodes

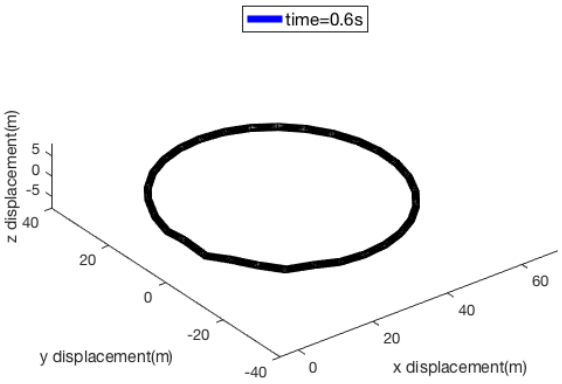


(b) Snapshot of collar (t=0.6s)

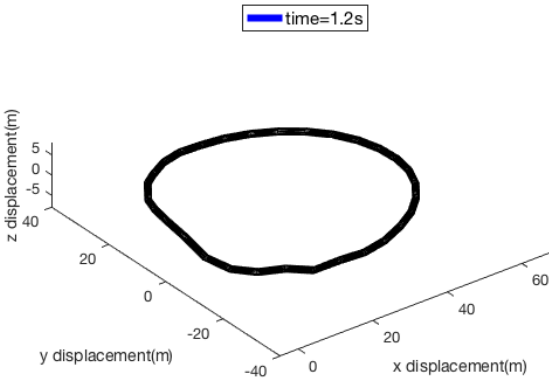


(c) Snapshot of collar (t=1.2s)

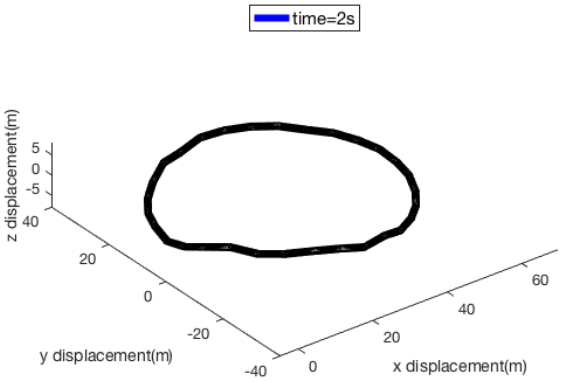


(d) Snapshot of collar (t=2.0s)

Figure 3.18: Collar drop from -3 to 3m of initial displacement

### 3.1.5 Summary of structural model validation

To sum up the validations with ANSYS as well as other reliable sources, it can be concluded that the structural solver has a capability to solve a dynamic beam equations with a great accuracy provided that a proper time step is given. Figure 3.19 and Figure 3.20 present maximum amplitude errors and average phase errors compared to ANSYS results for converged validations cases. Few cases not dealt with here did not show a convergence due to a coarse time step to calculate such a validation case. From these two summary figures, a general pattern is observed where the increased number of elements yields more accurate results. Another key finding is that a finer time step is required to get a similar level of accuracy in case of a larger number of elements. Thus, even higher computing resource is needed for a larger number of elements. That is why a proper number of elements should be decided before calculating dynamic beam equations.

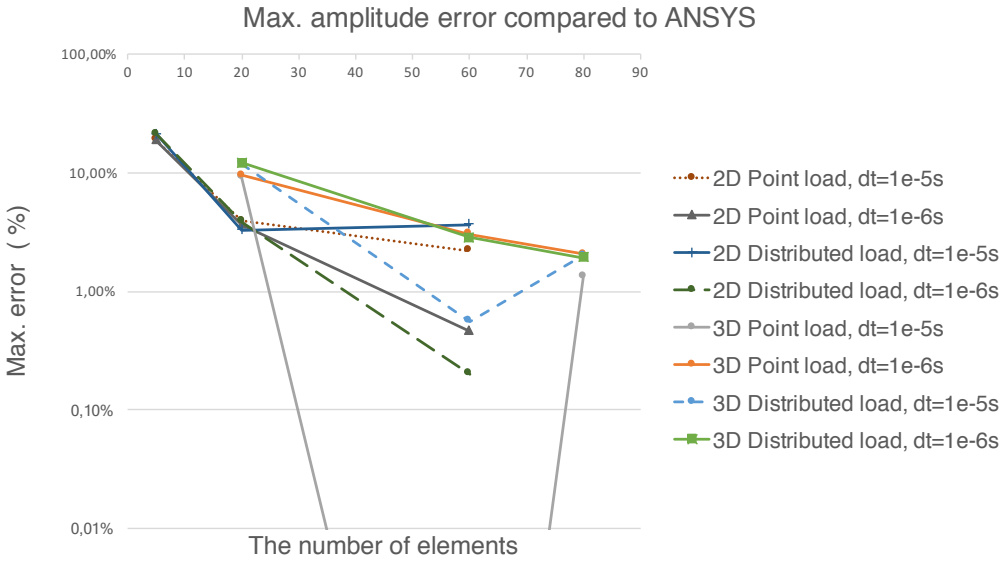


Figure 3.19: Summary of maximum amplitude error

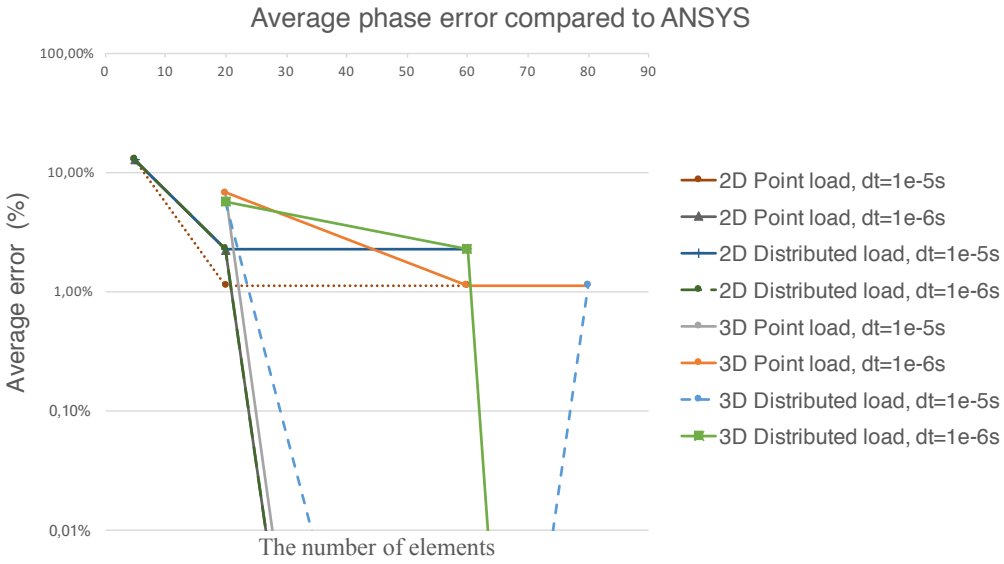


Figure 3.20: Summary of average phase error

## 3.2 Presentation of Fluid Model

This section will present the intermediate results from the prepared fluid model which will be used in fluid-structure interaction investigation for future work. Here, REEF3D is capable of calculating over 6 degree of freedom for the motion of a structure in waves and/or currents. In this section, the setups and results from the simulations performed on both 2-D cylinder and 3-D collar model are shown. As presented in Figure 3.21 and 3.26, the respective preparations for the simulations were set up. A numerical beach prevents wave reflections at the outlet of the tank in case waves are used in numerical wave tanks.

Firstly, it is necessary to verify the numerical domain and motions depicted by mesh. The procedure used in this presentation section follows the order of bulleted items below:

- Waves on a fixed structure
- Heave decay test of structure
- Waves on a free floating structure

To define mesh of the calculation domain an open source code DIVEMesh is used. For the post-processing of the calculation, ParaView is employed to visualise the physical quantities of the calculation domain and the behaviours of structures.

### 3.2.1 2-D cylinder model

A floating 3-D collar itself has a relatively complicated shape when it comes to a numerical calculation. There will be a lot of errors and difficulties if anyone tries to run directly the 3-D collar case without building up a relevant know-how and lessons learned. In order to save computational cost and efforts it is checked first that a simplified 2-dimensional object, which is a cylinder structure lain on the surface, is well prepared to be analysed.

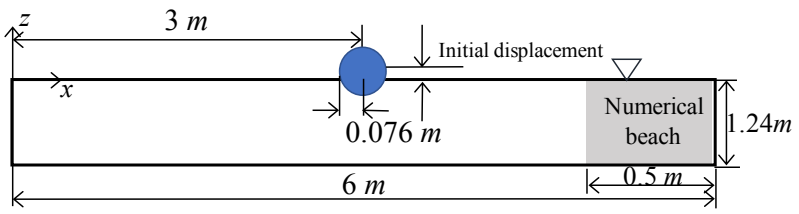


Figure 3.21: Numerical wave tank for 2-dimensional cylinder

#### 3.2.1.1 Simulation set-up

Table 3.7 tabulated the main parameters that are used in this presentation case. The numerical wave tank used in this simulation is 2 dimensional such that it has a single cell in $y$ direction. As illustrated in Figure 3.21 the numerical wave tank has 6 $m$ long and 1.24 $m$ of water depth. In case of wave action, 0.5 m of the numerical beach is applied in the leeward side of the cylinder.

Table 3.7: Input parameters for the numerical wave tank of the 2-D cylinder model

| Properties | Unit | Value | Properties | Unit | Value |
|---|---|---|---|---|---|
| Length | $m$ | 6 | Cylinder density | $kg/m^3$ | 500 |
| Width | $m$ | 0.02 | Cylinder radius | $m$ | 0.076 |
| Depth | $m$ | 2.48 | Wave height | $m$ | 0.06 / 0.2 |
| Water Depth | $m$ | 1.24 | Wave period | $m$ | 1.0 / 1.5 |
| Relaxation zone | $m$ | 0.5 | | | |
| Number of cells | - | 12 000 | | | |

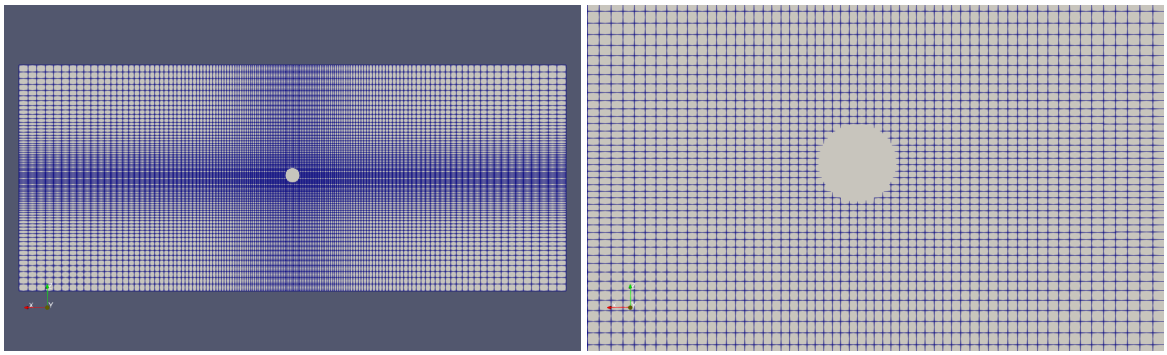

(a) Stretched calculation domain (b) Mesh grid around the cylinder

Figure 3.22: Numerical mesh for the 2-D cylinder model

As presented in Figure 3.22, the stretched mesh grid is applied both in $x$ and $z$ direction to refine the mesh around the solid structure. Accordingly, around 10 cells in x direction and 8 cells in z direction are prepared corresponding to the diameter of the cylinder since minimum cell side of $\Delta x = 0.01653$ $m$ and $\Delta z = 0.0128$ $m$ around the cylinder.

#### 3.2.1.2 Waves on fixed model

Firstly, the structure is fixed while waves are exerting on the structure. 2nd order Stokes wave is applied here and the parameters of the wave are stipulated in Table

3.7. A numerical beach is applied in downwind side of the cylinder. In REEF3D wave forces can be calculated.

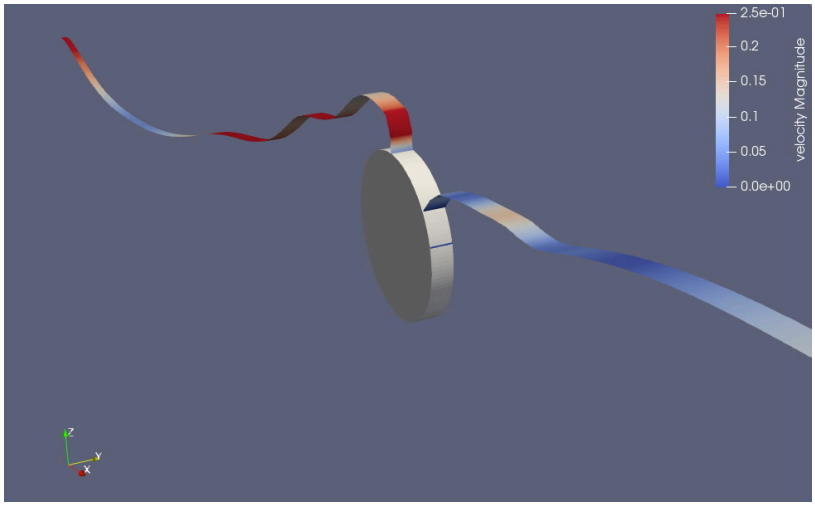


Figure 3.23: Waves on fixed 2-D cylinder (0.2m of wave height)

#### 3.2.1.3 Heave decay test

It is important to understand heave motions of floating structures in terms of period and damping action in that the structures and their support structures e.g. mooring line, are designed by such these input values. During the test, all sides of numerical wave tanks are bound by wall boundary without waves. In Figure 3.24, a small

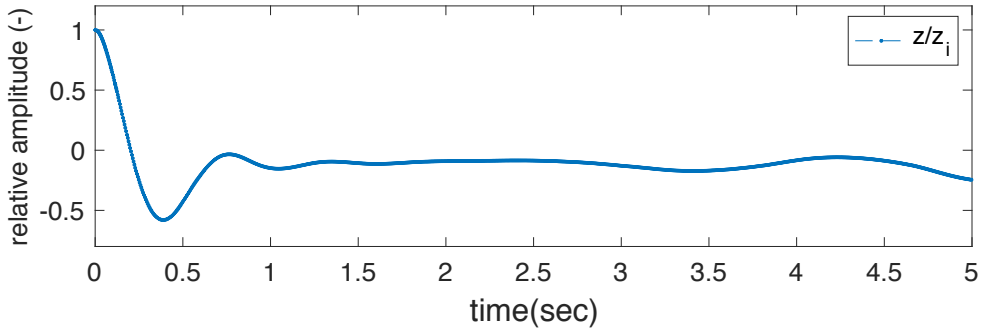


Figure 3.24: Heave decay test of the 2-D cylinder model

perturbation is observed after 4 seconds of elapsed time. It is recognised that the wall boundaries reflect the incoming waves made by the cylinder so that the reflected waves affect the cylinder again. To validate with any reliable source, this effect should be aware of and investigated how the reference dealt with these reflective waves.

#### 3.2.1.4 Waves on free floating 2-D cylinder

This presentation case allows heave and pitch motions of the 2-D cylinder in waves. 2nd order Stokes waves are generated with wave heights $H = 0.06\ m$ and $0.2\ m$ and wave period $T = 1.0\ s$ and $1.5\ s$, respectively. The motion of structure is captured with respect to its centre of gravity.

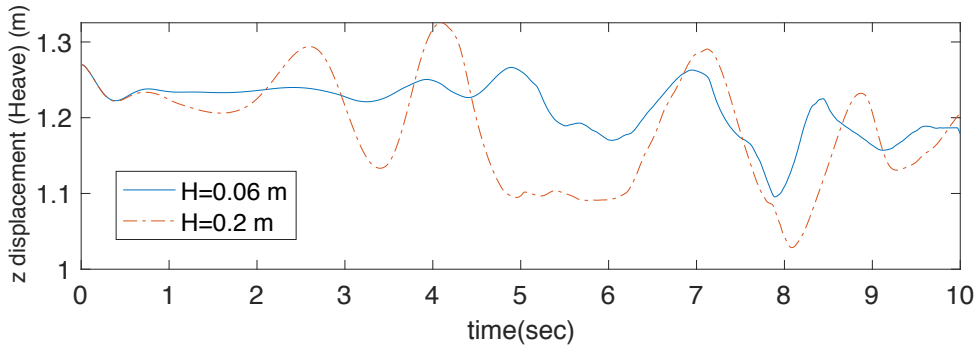


(a) Vertical position - z direction - of the cylinder

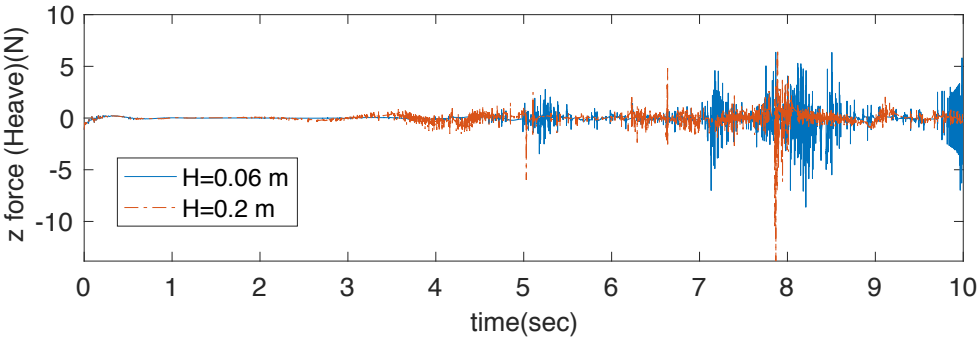


(b) Vertical force - z direction - for the cylinder model

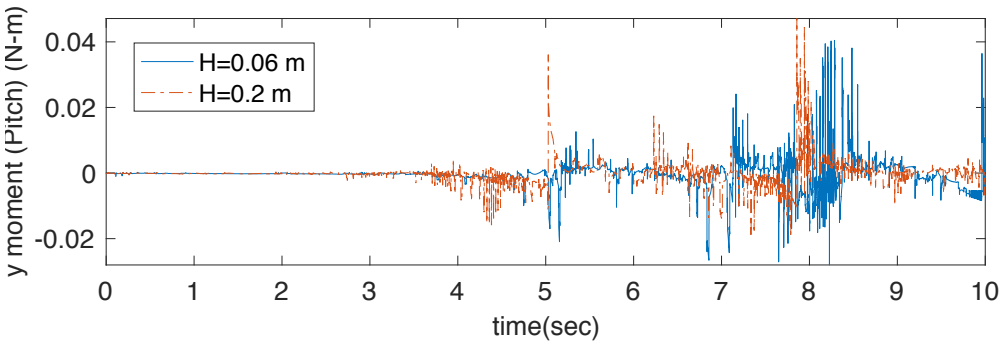


(c) Pitch moment- y axis - for the cylinder model

Figure 3.25: Positions and forces of the free floating 2-D cylinder

### 3.2.2 3-D collar model

Unlike the 2-D cylinder model presented above, 1:10 scaled model is applied in 3-D collar model. With the similarity, one can figure out the magnitude of physical quantities qualitatively and quantitatively compared to the actual structure the one is aiming for.

#### 3.2.2.1 Simulation set-up

The considered wave tank is 8 $m$ long, 1.5 $m$ high (0.75 $m$ water depth) and 8 $m$ wide. A floating collar of 5.73 $m$ diameter is placed inside the tank at ($x$,$y$,$z$) = ($4m$, $4m$, $0.75m$). Its cross section diameter is 0.15 $m$ and the density is 811.8 $kg/m^3$. The incoming waves are regular 2nd order Stokes waves and have a height of 0.06, 0.5 and 1.0 $m$, a period T = 1 , 2 and 4 $s$, respectively.

Table 3.8: Input parameters for the numerical wave tank of the 3-D collar model

| Properties | Unit | Model value | Actual value |
|---|---|---|---|
| Length | $m$ | 8 | 80 |
| Width | $m$ | 8 | 80 |
| Depth | $m$ | 1.5 | 15 |
| Water Depth | $m$ | 0.75 | 7.5 |
| Relaxation zone | $m$ | 0.5 | 5 |
| Number of cells | - | 4 485 000 | - |
| Wave height | $m$ | 0.06 / 0.12 / 0.18 | 0.6 / 1.2 / 1.8 |
| Wave period | $m$ | 1.0 / 1.5 / 1.8 | 3.16 / 4.74 / 5.69 |

Table 3.9: Input parameters for the collar structure model

| Properties | Unit | Model value | Actual value |
|---|---|---|---|
| Collar density | $kg/m^3$ | 811.8 | 811.8 |
| Collar cross section diameter | $m$ | 0.15 | 1.5 |
| Volume | $m^3$ | 0.293871 | 293.871 |
| Mass | $kg$ | 238.565 | 238 565 |
| Mass moment of inertia (Ixx / Iyy) | $kgm^2$ | 978.95 | 97 895 211 |
| Mass moment of inertia (Izz) | $kgm^2$ | 1957.90 | 195 790 422 |

Table 3.8 and 3.9 summarise the main parameters that are used in this presentation case. In case of wave action similar to 2-D cylinder model, 0.5 m of numerical beach is applied in the leeward side of the collar. The mesh of calculation domain is refined

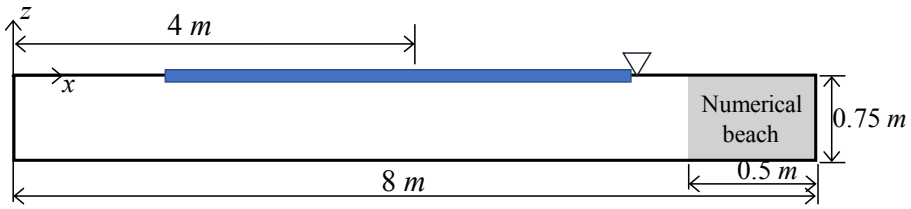


Figure 3.26: A schematic drawing for a collar model set-up in the numerical wave tank

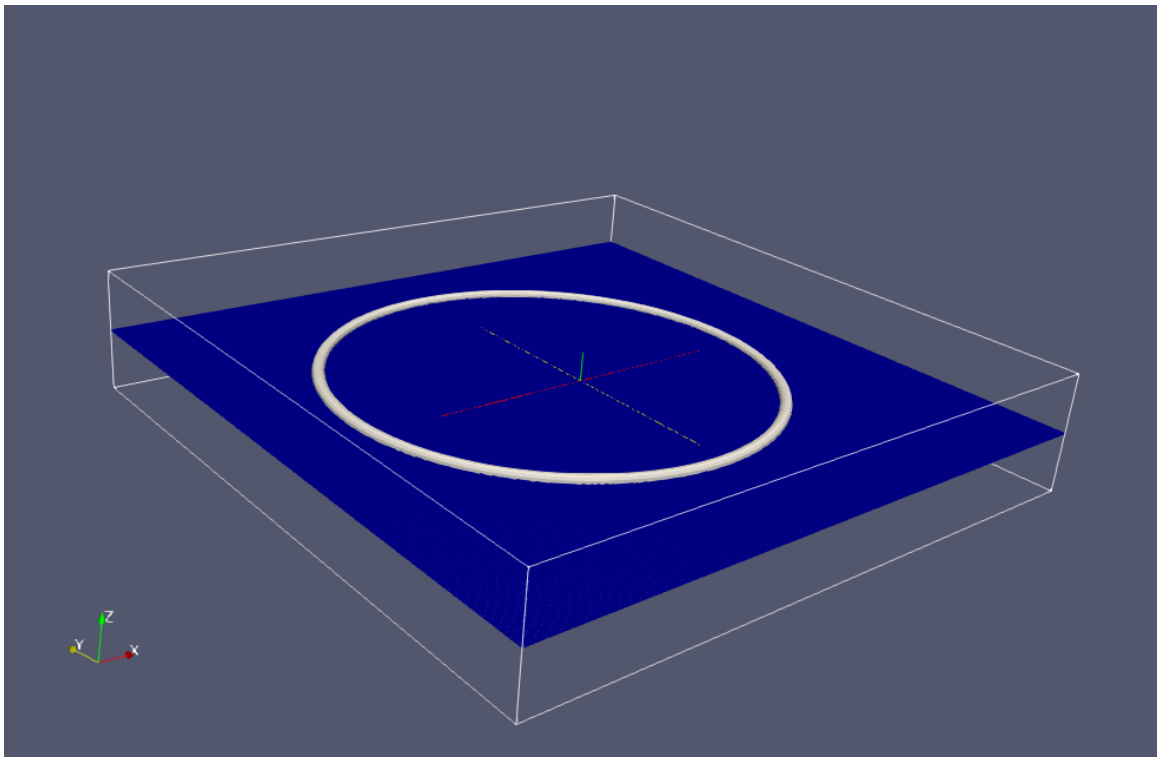

Figure 3.27: A perspective view of the numerical wave tank for 3-D collar model

by equidistant size of mesh in all the direction so that around maximum 5 to 6 cells in all the directions are prepared corresponding to the diameter of the collar cross section. Here, the minimum $\Delta x = 0.027\ m$, $\Delta y = 0.027\ m$ and $\Delta z = 0.03\ m$ over the domain.

It has been suggested in Section 2.2.6.3 that an extreme wave loading is eventually applied for verifying a limiting case in terms of the structural design. However, this study establishes the basis for the advanced investigation of the fluid-structure interaction and its effects on the design. Thus, a relative small wave heights are assumed and applied by an engineering judgement as presented in Table 3.8.

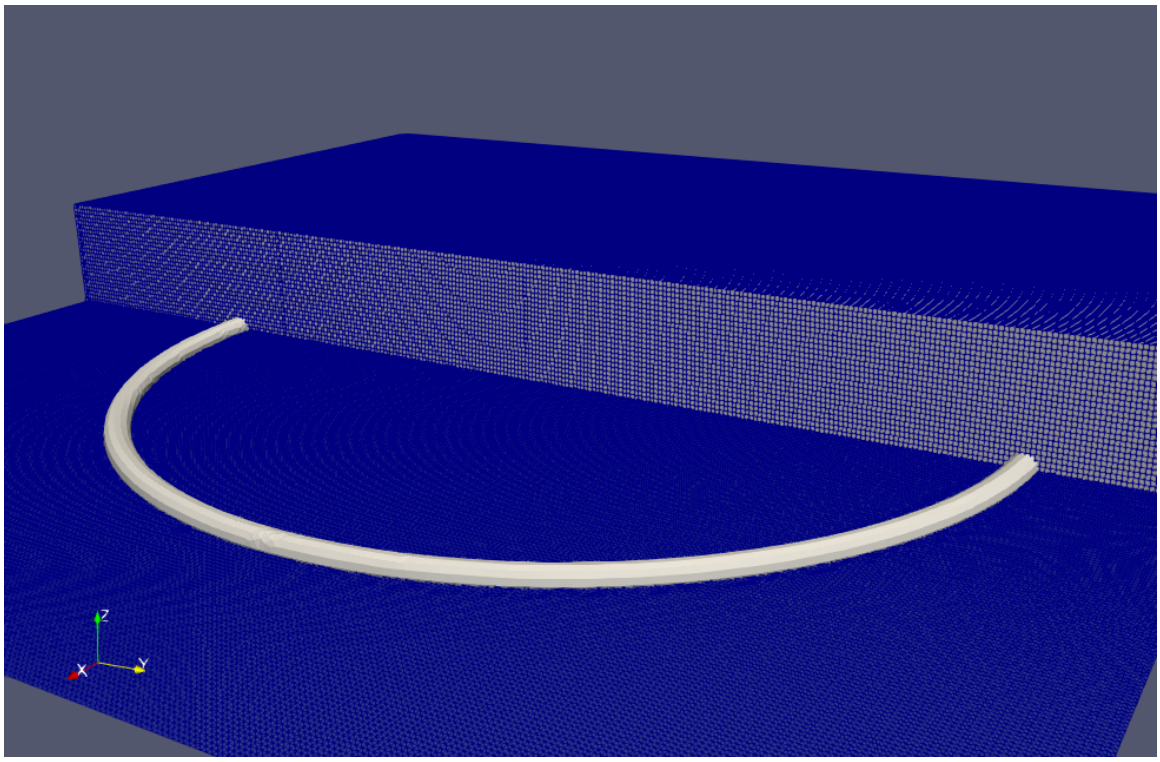

Figure 3.28: A perspective view (a cut by profile) of the calculation domain

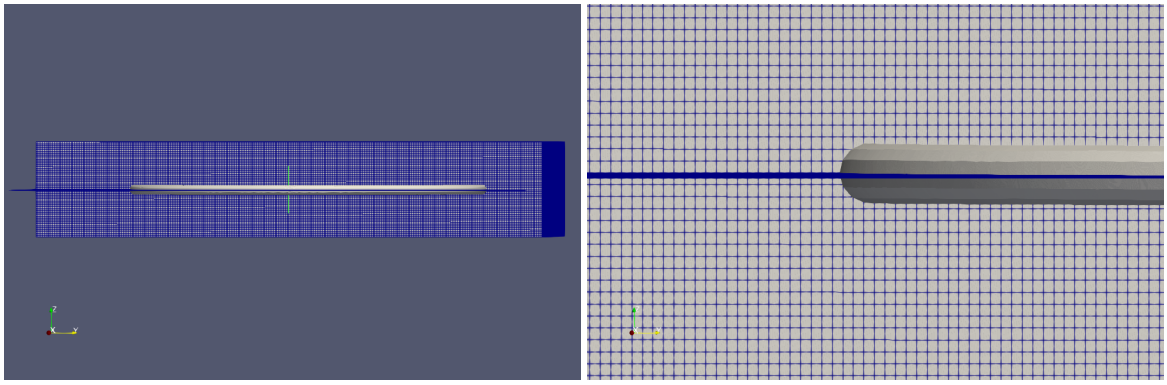

(a) Mesh grids for calculation domain (b) Mesh grid around the cylinder

Figure 3.29: Numerical mesh for the 3-D collar model

#### 3.2.2.2 Waves on fixed model

The collar model is fixed on the initial location and 2nd order Stokes waves were generated and acting on the structure. The wave heights and periods are stipulated in Table 3.8. From the results of the wave forces, it is observed that the forces increase nonlinearly for all kinds of components as the wave height increases.

Considering the scale ratio is 1:10, the magnitude of lift force and drag force would

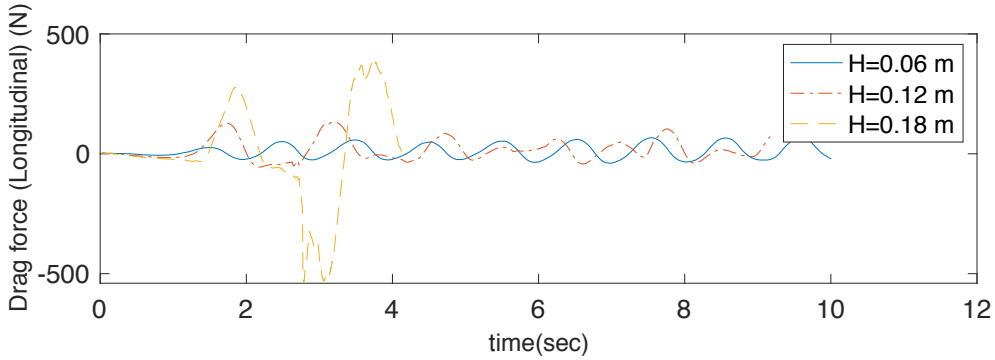


(a) Longitudinal force - x direction - for the collar model

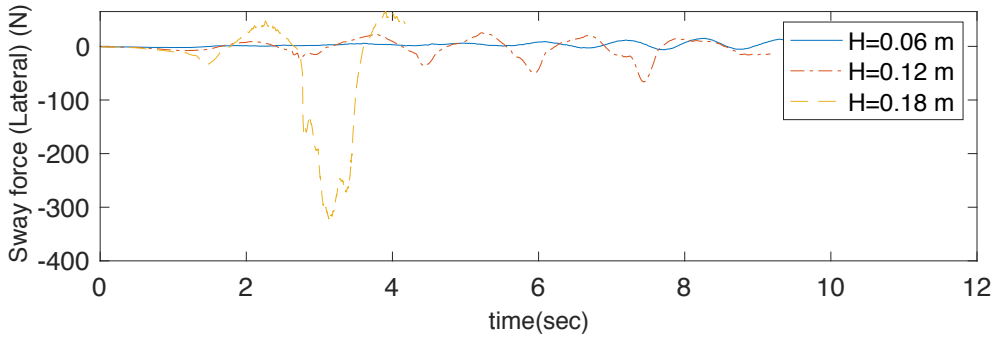


(b) Lateral force - y direction - for the collar model

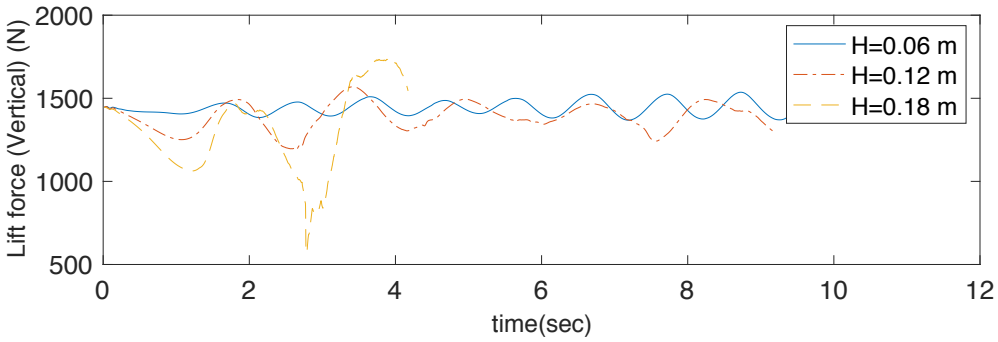


(c) Vertical force - z direction - for the collar model

Figure 3.30: Wave forces on the 3-D collar model

be the order of 1 000 000 $N$ and 500 000 $N$ in actual scale. Thus, these values can be an input value, for instance, to inaugurate the design process if this calculation becomes more quantitatively reliable by validating the results.

#### 3.2.2.3 Heave decay test

On heave test for the 3-D collar model, two different initial displacements were applied, 0.05 $m$ and 0.14 $m$, as plotted in Figure 3.31.

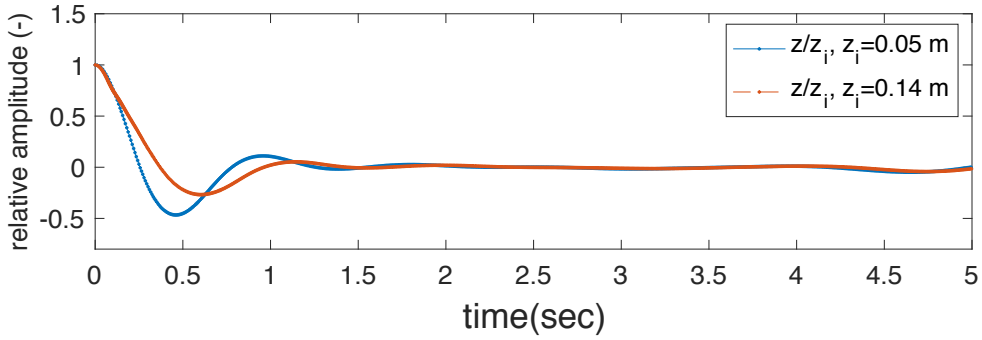


Figure 3.31: Heave decay test of the 3-D collar model

Similarly, 3-D collar model has a small perturbation observed after 4 seconds of elapsed time as 2-D cylinder case had. Since all the sides of numerical wave tanks are bounded by wall boundary, generated waves by the heave motion have been reflected and have interrupted the structure again.

#### 3.2.2.4 Waves on free floating 3-D collar

Lastly, this simulation concerns two motions out of 6 degree of freedom of the floating collar model. Surge and heave motions are allowed in the simulation, which are longitudinal - $x$ direction - and vertical - $z$ direction - components both in displacements and in forces.

In Figure 3.32, a small initial displacement in heave was observed and the displacement had decayed as time goes by. The surge forces were fluctuating irregularly while the displacement roses due to Stokes drift.

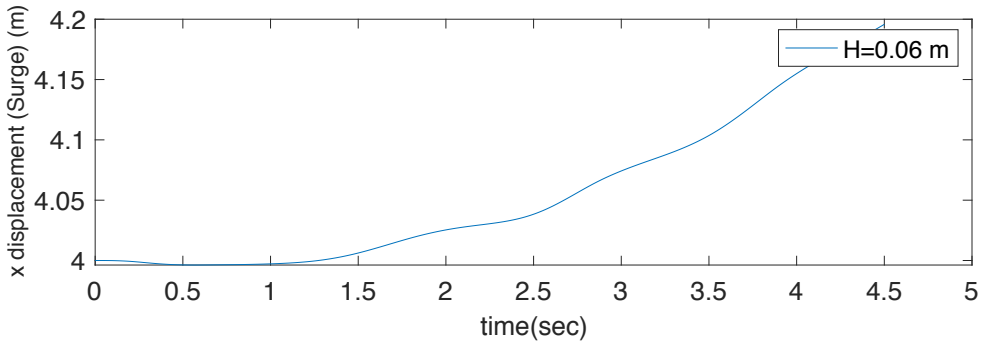


(a) Longitudinal displacement (Surge) - for free floating collar

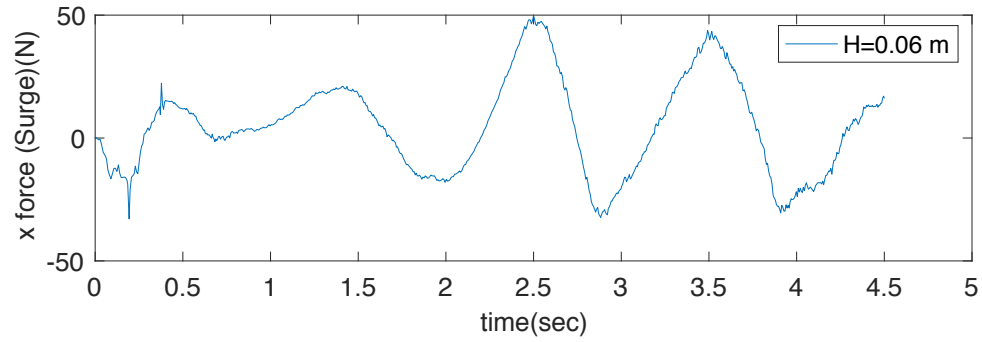


(b) Longitudinal force (Surge) - for free floating collar

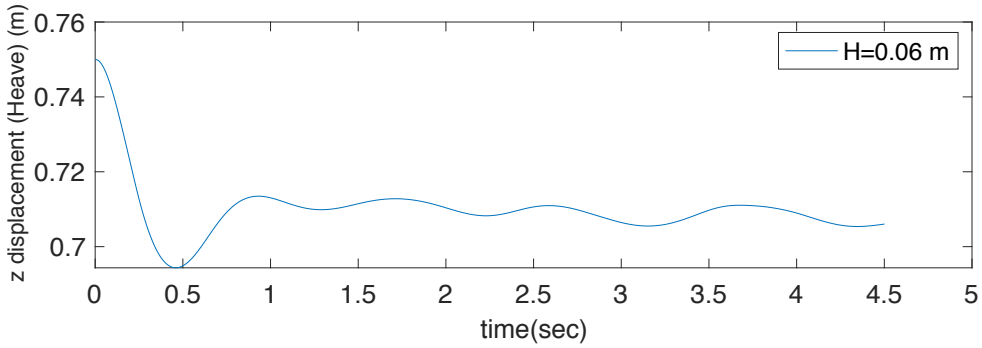


(c) Vertical displacement (Heave) for free floating collar

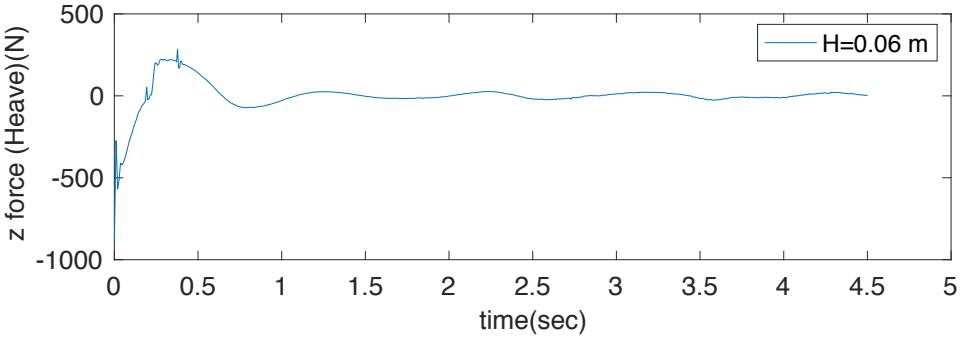


(d) Vertical force (Heave) for free floating collar

Figure 3.32: Surge and heave displacement and forces on the 3-D collar model

# Chapter 4

# Conclusions

In this thesis a structure solver has been introduced for the collar modelling using a 3-D beam model. The solver handles the dynamic beam equation by which one could have a basis for FSI model that interact with fluid in both ways. Indeed, this will be another capable feature from REEF3D.

## 4.1 Key Findings and Discussions

To summarise the work done by this thesis, the significant findings are observed as below:

- The FEM Solver showed a good agreement in validation with other reliable sources providing a high accuracy given that a proper time step is chosen.
- The number of element is one of parameters to determine the accuracy of the numerical schemes so that a finer time step is required in a larger number of element to acquire a certain level of accuracy.
- The required time step is a function of stiffness in general Newmark family schemes.
- The fluid model proved that REEF3D has a capability to calculate a torus shaped collar model in waves both in fixed position and in floating state of the model.

In conclusion, the following discussion can be followed for the structure model and the fluid model. Firstly, for the structural model:

- Newmark scheme is unconditionally stable but not always accurate that is why a collection of verifications needs to be performed to determine a proper time step for a specific case.

- Appropriate number of elements should be selected considering computational cost and the accuracy of the numerical solution.

Secondly, the fluid model should be optimised considering the following:

- Configurations of different cell sizes and their effects on the results
- How boundary condition affect the results and the structure to validate an experimental results or another reliable calculations.
- Presenting of extremes wave case which would limit the structure design
- Finite water depth and its effects on wave propagations compared to actual aquaculture sites since in this thesis a very shallow water depth is employed to reduce the computational cost.

## 4.2 Future Work

Based on this thesis work, the next step is to construct a coupling model where both structural solver and fluid solver are integrated. The coupling model can be explained by the work flow in the figure 4.1, presenting fluid-structure interaction.

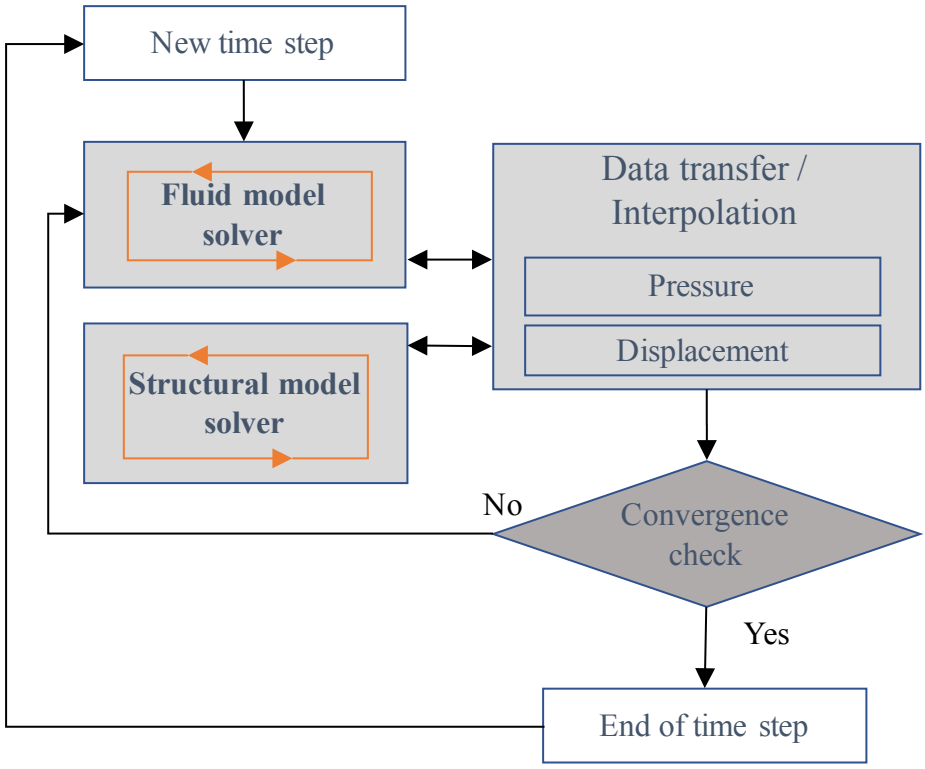


Figure 4.1: The work flow of analysis for fluid-structure interaction

From the work flow, for a certain time, displacements calculated by both solvers should be agreed within a tolerance, otherwise, another iteration will be performed for the displacements to converge from either solvers. To evaluate each iterative computation, a data transfer and a convergence check feature should be prepared as already mentioned, where the common surface information has been formed by a stl format, which requires trianglarized meshes. Also, an interpolation function is required to estimate unknown values due to a different reference point between two numerical models.

# Appendix A

# FEM Solver Documentation

## A.1 m-files and functions

Execution m-file (Collar_r7.m)

```
%% Calculate the torus collar
clear all; clc; close all;
Q2=FECase;
Q2.TotalLength=18; % Circumference length
Q2.op=2; % Transient analysis=2 , Static analysis =1
Q2.Dimension=3; %Dimension; 3D Beam (BEAM4 in Ansys) = 3, 2D Beam (BEAM3
in Ansys) = 2
Q2.NumMethod=1; %Newmark=1, Runge-Kutta(ode45)=2, no more used
Q2.D=0.15; % Diameter of circle
Q2.op2=2; % connectivity = Closed circle
Q2.tend=0.2; %the end of simulation time
% Initialise parameter and default inputs
Q2=initialise_FECase(Q2,30);
Q2.K = Assemble_K(Q2);
Q2.M = Assemble_M(Q2);
dt=0.001;
% Main Calculation by Newmark method
tt2,u2
=cal_FEM(Q2,dt);
%% Plot the time series
figure(2),
plot(tt2,u2(2,:),'-ob','DisplayName',sprintf('First node %dD-Beam,
n= %d, dt= %e', Q2.Dimension, Q2.nele, dt),'MarkerSize',3,'LineWidth',2);
hold on;
```

```
plot(tt2,u2(8,:),'-.k','DisplayName',sprintf('Second node %dD-Beam,
n= %d, dt= %e', Q2.Dimension, Q2.nele, dt),'MarkerSize',3,'LineWidth',2);
hold on;
plot(tt2,u2(Q2.ndof-10,:),'--r','DisplayName',sprintf('Last
node %dD-Beam, n= %d, dt= %e', Q2.Dimension, Q2.nele,
dt),'MarkerSize',3,'LineWidth',2);
legend('-DynamicLegend','FontSize',12);
legend show;

axis([0 1.0 -5.0 5.0]);
set(gcf, 'Position', [100, 100, 500, 300])
set(gca,'FontSize',13)
title('HDPE torus, initial displacement = -3 to 3(m)','FontSize',16)
xlabel('time(sec)','FontSize',15);
ylabel('displacement(m)','FontSize',15);

%% 3D Plot (GIF)
% this function takes some time to run, of course it is depending on the
% machine condtion and the number of meshes
plot_collar(Q2,u2,dt);
```

FECase.m

```
classdef FECase
properties
Dimension; NumMethod; nele; ndof; dof; EAe; EIe; EIye; Le; alphae;
phie;thetae;
load; %nodal load
loadf; %function type load
load_backup;
elload; %element load on midspan
elloadf; %function type element load
support;
displ;
KeL;
K; MeL; M; rho; Ar; Ay; Ir; Ix; Iy; tspan; dt; op; op2; ec; D; Di; t;
YM; PR; G; Jx; TotalLength; total_displ; total_t; g; rhow; tend; th;
end
end
%%
```

Assemble_K.m

```
function K=Assemble_K(obj_)
K = zeros(obj_.ndof);
for i=1:obj_.nele
R=R_mat(obj_.alphae(i),obj_.phie(i),obj_.thetae(i),obj_.Dimension);
RT=R.';
Ke(:,:,i)=RT*obj_.KeL(:,:,i)*R;
for j=1:obj_.dof
for k=1:obj_.dof
K(obj_.ec(i,j),obj_.ec(i,k))=K(obj_.ec(i,j),obj_.ec(i,k))
+Ke(j,k,i);
end
end
end
if obj_.op2==2 % Reduce last 6 degree of freedom for Enclosed type of
beam since last node = first node
N=(obj_.dof/2)*(obj_.nele);
K(:,N+1:N+6)=[];
K(N+1:N+6,:)=[];
end
end
```

Assemble_M.m

```
function M=Assemble_M(obj_)
M=zeros(obj_.ndof);
for i=1:obj_.nele
R=R_mat(obj_.alphae(i),obj_.phie(i),obj_.thetae(i),obj_.Dimension);
RT=R.';
Me(:,:,i)=RT*obj_.MeL(:,:,i)*R;
for j=1:obj_.dof
for k=1:obj_.dof
M(obj_.ec(i,j),obj_.ec(i,k))=M(obj_.ec(i,j),obj_.ec(i,k))+Me(j,k,i);
end
end
end
```

```
if obj_.op2==2 % Reduce last 6 degree of freedom for Enclosed type of
beam since last node = first node
N=(obj_.dof/2)*(obj_.nele);
M(:,N+1:N+6)=[];
M(N+1:N+6,:)=[];
end
end
```

Cal_FEM.m

```
function [tt,u]=cal_FEM(obj_,dt)
for i=1:obj_.nele % only for initial condition!!  don't make a comment
line

R=R_mat(obj_.alphae(i),obj_.phie(i),obj_.thetae(i),obj_.Dimension);
RT=R.';
feqLq, feqLF
=eqL(obj_.Le(i),obj_.elload(i,1),obj_.elload(i,2),obj_.Dimension);
feqq=RT*feqLq';
feqF=RT*feqLF';
Fe(i,:)=zeros([1 obj_.dof]);
Fe(i,:)=Fe(i,:)+feqq'+feqF';
for j=1:obj_.dof
obj_.load(1,obj_.ec(i,j))=obj_.load(1,obj_.ec(i,j))+Fe(i,j);
end
end
if obj_.op2==2 %Torus(ring) shape
obj_.load(:,obj_.ndof-5:obj_.ndof)=[];
end
if obj_.op==2 % Dynamic
u0=zeros([1 obj_.ndof]);
ud0=zeros([1 obj_.ndof]);
N=obj_.nele+1;
if obj_.op2==2
u0=zeros([1 obj_.ndof-6]);
ud0=zeros([1 obj_.ndof-6]);
N=obj_.nele;
end
%%% Initial displacement input here !!!!!!!  for collar drop case only
```

```
for i=1:N
u0(1,2+(i-1)*6)=0;%-3+i*0.2;
end

tt,u
=Newmark(dt,obj_.tspan(end),u0,ud0,obj_.M_.load',obj_.load,obj_);
%Newmark(dt,tmax,u0,ud0,udd0,ndof,f0,M,K)

else % Static analysis
for i=1:obj_.ndof
if obj_.support(i)==1
for j=1:length(obj_.support)
obj_.K(i,j)=0.0;
obj_.K(j,i)=0.0;
end
obj_.K(i,i)=1.0;
end
end
u=obj_.K_.load';
tt=0;
for i=1:obj_.ndof
if obj_.support(i)==1
u(i)=0.0;
end
end
end
end
```

eqL.m

```
function [feqLq_, feqLF_]=eqL(L_, q_, F_,dimension_)
%This function evaluates equivalent distributed loads and nodal forces
if dimension_==3
feqLq_=[0 (1/2)*q_*L_ 0 0 0 -(1/12)*q_*L_.^2 0 (1/2)*q_*L_ 0 0 0
(1/12)*q_*L_.^2];
feqLF_=[0 F_/2 0 0 0 -F_*L_/8 0 F_/2 0 0 0 F_*L_/8];
else
feqLq_=[0 (1/2)*q_*L_ -(1/12)*q_*L_.^2 0 (1/2)*q_*L_ (1/12)*q_*L_.^2];
feqLF_=[0 F_/2 -F_*L_/8 0 F_/2 F_*L_/8];
end
end
```

GetMeshPoint.m

```
function pm=GetMeshPoint(p0,p1,Di)
delp=p1-p0;
ps0=[delp(1) delp(2) delp(3)+Di/2];
% finding perpendicular vectors of element axis
h=null((ps0').');
pv=(h(:,1)'/norm(h(:,1)));
ph=(h(:,2)'/norm(h(:,2)));

pv1=rodrigues_rot(pv,delp,pi/4);
ph1=rodrigues_rot(ph,delp,pi/4);
pv2=rodrigues_rot(pv,delp,pi);
ph2=rodrigues_rot(ph,delp,pi);
pv3=rodrigues_rot(pv,delp,5*pi/4);
ph3=rodrigues_rot(ph,delp,5*pi/4);

pv4=rodrigues_rot(pv,delp,pi/8);
ph4=rodrigues_rot(ph,delp,pi/8);
pv5=rodrigues_rot(pv,delp,3*pi/8);
ph5=rodrigues_rot(ph,delp,3*pi/8);
pv6=rodrigues_rot(pv,delp,9*pi/8);
ph6=rodrigues_rot(ph,delp,9*pi/8);
pv7=rodrigues_rot(pv,delp,11*pi/8);
ph7=rodrigues_rot(ph,delp,11*pi/8);
% Basically 32 mesh points per node, which means 11.25 degree between
two
% mesh points when we look at the section of one node

pm(1,:)=p0+Di/2*pv; pm(2,:)=p0+Di/2*pv4; pm(3,:)=p0+Di/2*pv1;
pm(4,:)=p0+Di/2*pv5; pm(5,:)=p0+Di/2*ph; pm(6,:)=p0+Di/2*ph4;
pm(7,:)=p0+Di/2*ph1; pm(8,:)=p0+Di/2*ph5; pm(9,:)=p0+Di/2*pv2;
pm(10,:)=p0+Di/2*pv6; pm(11,:)=p0+Di/2*pv3; pm(12,:)=p0+Di/2*pv7;
pm(13,:)=p0+Di/2*ph2; pm(14,:)=p0+Di/2*ph6; pm(15,:)=p0+Di/2*ph3;
pm(16,:)=p0+Di/2*ph7;
end
```

Newmark.m

```
function [t,u]=Newmark(dt,tmax,u0,ud0,udd0,f0,obj_)
fileID = fopen('load.txt','w');
fileID2 = fopen('Force.txt','w');
fprintf(fileID,'time(s) node load(N)');
fprintf(fileID2,'time node force(N) stress(N/m2)');
fileID=fopen('load.txt','a+');
fileID2=fopen('Force.txt','a+');

delta=0.5;
alpha=0.25*(0.5+delta)^2;
t=0:dt:tmax;disp(t);
if obj_.op2==2
N=obj_.ndof-6;
else
N=obj_.ndof;
end
u=zeros(N,length(t));u(:,1)=u0;
fh=zeros(N,length(t));fh(:,1)=f0;
ud=zeros(N,length(t));ud(:,1)=ud0;
udd=zeros(N,length(t));udd(:,1)=udd0;
a0=1/alpha/dt^2;
% a1=delta/alpha/dt; %Not used here
a2=1/alpha/dt;
a3=1/2/alpha-1;
% a4=delta/alpha-1; %Not used ahere
% a5=dt/2*(delta/alpha-2); %Not used here
a6=dt*(1-delta);
a7=delta*dt;
Kh=obj_.K+a0*obj_.M; % Damping coefficient=0

for k=1:N
if obj_.support(k)==1
u(k,1)=0.0;
end
end
fhe=fh;
for i=1:length(t)-1
if t(i)<0.0
% fh(obj.ndof-4,i)=-0.1; % in case forcing within a second
% fh(:,i)=0;
```

```
else % Make a comment line when cantilever validations
% % if functional load e.g.  time vairant, should be defined here inside
% % in case constant load, this definition can be waste of time.
obj_.load = zeros([1 N]);
for j=1:obj_.nele
z1=u(2+(obj_.dof/2)*(j-1),i);
if (2+(obj_.dof/2)*(j))>N
z2=u(2,i);
else
z2=u(2+(obj_.dof/2)*(j),i);
end
zz=(z1+z2)/2;
Az=real(2*obj_.D^2/4*(asin(zz/(obj_.D/2))+0.5*sin(2*asin(zz/(obj_.D/2)))));
obj_.elload(j,1)=-obj_.rhow*obj_.g*Az;
R=R_mat(obj_.alphae(j),obj_.phie(j),obj_.thetae(j),obj_.Dimension);
RT=R.';
feqLq, feqLF
=eqL(obj_.Le(j),obj_.elload(j,1),obj_.elload(j,2),obj_.Dimension);
feqq=RT*feqLq';
feqF=RT*feqLF';
Fe(j,:)=zeros([1 obj_.dof]);
Fe(j,:)=Fe(j,:)+feqq'+feqF';
% Printing load calculated by initial displacement
for k=1:obj_.dof
obj_.load(1,obj_.ec(j,k))=obj_.load(1,obj_.ec(j,k))+Fe(j,k);
fprintf(fileID,'%8.4f %d %8.4f',i,j,obj_.load(1,obj_.ec(j,k)));
end
end
fh(:,i)=obj_.load; % don't make a comment line

end
fhe(:,i+1)=fh(:,i)+(obj_.M*(a0*u(:,i)+a2*ud(:,i)+a3*udd(:,i)));
u(:,i+1)=Kh(:,i+1);

%%% This 5 lines below are necessary but it is waste of time for no %
boundary condition
for k=1:obj_.ndof
if obj_.support(k)==1
u(k,i+1)=0.0;
end
end
```

```
% Bathe (1982)
udd(:,i+1)=a0*(u(:,i+1)-u(:,i))-a2*ud(:,i)-a3*udd(:,i);
ud(:,i+1)=ud(:,i)+a6*udd(:,i)+a7*udd(:,i+1);

% % printing nodal forces / stresses
F2(:,i)=obj_.K*u(:,i);
S2(:,i)=F2(:,i)/obj_.Ar(1); % Assuming that each cross section area is
identical throught all the element
for j=1:N
fprintf(fileID2,'%d %d %e %e',i,j,F2(j,i),S2(j,i));
end
end
fclose(fileID2);
end
```

initialise_FECase.m and plot_collar.m are not included here.

# Bibliography


[1] K. Bathe. *Finite Element Procedures in Engineering Analysis*. PRENTICE-HALL, INC., Englewood Cliffs, New Jersey 07632, 1982.

[2] H. Bihs, A. Kamath, M. A. Chella, A. Aggarwal, and Ø. A. Arntsen. A new level set numerical wave tank with improved density interpolation for complex wave hydrodynamics. *Computers  Fluids*, 140:191–208, 2016.

[3] F. Cardia and A. Lovatelli. Aquaculture operations in floating hdpe cages - a field handbook. Technical report, FAO FISHERIES AND AQUACULTURE TECHNICAL PAPER, 2015.

[4] M. Chella. Breaking wave characteristics and breaking wave forces on slender cylinders. *PhD thesis*, 2016.

[5] A. J. Chorin. Numerical solution of the navier-stokes equations. *Mathematics of Computation*, 22:745–762, 1968.

[6] D. W. Fredriksson, M. R. Swift, O. Eroshkin, I. Tsukrov, J. D. Irish, and B. Celikkol. Moored fish cage dynamics in waves and currents. *IEEE JOURNAL OF OCEANIC ENGINEERING*, 30(1):251–270, 2005.

[7] D. W. Fredriksson, M. R. Swift, J. D. Irish, and B. Celikkol. The heave response of a central spar fish cage. *Proceedings of OMAE'02 21st International Conference on Offshore Mechanics and Arctic Engineering, June 23-28, Oslo, Norway*, 2002.

[8] A. Harten. High resolution schemes for hyperbolic conservation laws. *Journal of Computational Physics*, 49:357–393, 1983.

[9] A. Harten, B. Engquist, S. Osher, and S. Chakravarthy. Uniformly high order accurate essentially non-oscillatory schemes. *Journal of Computational Physics*, 71:231–303, 1987.

[10] C.-C. Huang, H.-J. Tang, and J.-Y. Liu. Effects of waves and currents on gravity-type cages in the open sea. *Aquacultural Engineering*, 38:105–116, 2008.

[11] Ø. Jensen, T. Dempster, E. B. Thorstad, I. Uglem, and A. Fredheim. Escapes of fish from norwegian sea-cage aquaculture: causes, consequences, prevention. *Aquaculture Environment Interactions*, 1:71–83, 2010. cited from the source : www.forskningsradet.no.

[12] G. S. Jiang and D. Peng. Weighted eno schemes for hamilton-jacobi equations. *SIAM Journal on Scientific Computing*, 21:2126–2143, 2000.

[13] A. Kamath. Cfd based investigation of wave-structure interaction and hydrodynamics of an oscillating water column device. *PhD thesis*, 2015.

[14] A. Kamath, M. A. Chella, H. Bihs, and Ø. A. Arntsen. Evaluating wave forces on groups of three and nine cylinders using a 3d numerical wave tank. *Engineering Applications of Computational Fluid Mechanics*, 9:343–254, 2015.

[15] S. Kleiven, P. Halldin, and D. Zenkert. Dynamic finite element methods. 2001. Lecture notes for SD2450 Biomechanics and Neuronics.

[16] P. Kohnke. Ansys theory reference release 5.6 eleventh edition. Technical report, 1999.

[17] T. Kristiansen and O. M. Faltinsen. Experimental and numerical study of an aquaculture net cage with floater in waves and current. *Journal of Fluids and Structures*, 54:1–26, 2015.

[18] H. E. Krogstad and Ø. A. Arntsen. *Linear Wave Theory Part A Regular Waves (Compandium)*. Norwegian University of Science and Technology, Trondheim, NORWAY, 2000.

[19] T. Martin, A. Kamath, and H. Bihs. Modelling and simulation of moored-floating structures using the tension-element-method. *Proceedings of the ASME 2018 37th International Conference on Ocean, Offshore and Arctic Engineering OMAE2018*, 2018.

[20] C. W. Shu and S. Osher. Efficient implementation of essentially non-oscillatory shock capturing schemes. *Journal of Computational Physics*, 717:439–471, 1988.

[21] I. Tsukrov, O. Eroshkin, D. Fredriksson, M. Swift, and B. Celikkol. Finite element modeling of net panels using a consistent net element. *Ocean Engineering*, 30:251–270, 2003.

[22] F. Vikeb, T. Furevik, G. Furnes, N. G. Kvanst, and M. Reistad. Wave height variations in the north sea and on the norwegian continental shelf, 1881-1999. *Continental Shelf Research*, 23:251–263, 2003.

[23] R. Wiebe and I. Stanciulescu. Inconsistent stability of newmark's method in structural dynamics applications. *J. Comput. Nonlinear Dynam*, 10(5).

[24] T. Xu, H. Hou, G. Dong, Y. Zhao, and W. Guo. Structural analysis of float collar for metal fish cage in waves. *Turkish Journal of Fisheries and Aquatic Science*, 17:257–268, 2017.

[25] T. Yokoyama. Vibrations of a hanging timoshenko beam under gravity. *Journal of Sound and Vibration*, 141(2):245–258, 1990.